CrossMark

ORIGINAL PAPER

Protracted, coeval crust and mantle melting during Variscan late-orogenic evolution: U–Pb dating in the eastern French Massif Central

Oscar Laurent[1,2,12] · Simon Couzinié[3,4] · Armin Zeh[1,5] · Olivier Vanderhaeghe[6] ·
Jean-François Moyen[3] · Arnaud Villaros[7,8,9] · Véronique Gardien[10] ·
Cyril Chelle-Michou[3,11]

Abstract The late stages of the Variscan orogeny are characterized by middle to lower crustal melting and intrusion of voluminous granitoids throughout the belt, which makes it akin to "hot" orogens. These processes resulted in the development of large granite–migmatite complexes, the largest of which being the 305–300-Ma-old Velay dome in the eastern French Massif Central (FMC). This area also hosts a wide range of late-Variscan plutonic rocks that can be subdivided into four groups: (i) cordierite-bearing peraluminous granites (CPG); (ii) muscovite-bearing peraluminous granites (MPG); (iii) K-feldspar porphyritic, calc-alkaline granitoids (KCG) and (iv) Mg–K-rich (monzo) diorites and lamprophyres ("vaugnerites"). New results of LA-SF-ICP-MS U–Pb zircon and monazite dating on 33 samples from all groups indicate that both granites and

mafic rocks emplaced together over a long period of ~40 million years throughout the Carboniferous, as shown by intrusion ages between 337.4 ± 1.0 and 298.9 ± 1.8 Ma for the granitoids, and between 335.7 ± 2.1 and 299.1 ± 1.3 Ma for the vaugnerites. Low zircon saturation temperatures and abundant inherited zircons with predominant late Ediacaran to early Cambrian ages indicate that the CPG and MPG formed through muscovite or biotite dehydration melting of ortho- and paragneisses from the Lower Gneiss Unit. The KCG and vaugnerites contain very few inherited zircons, if any, suggesting higher magma temperatures and consistent with a metasomatized lithospheric mantle source for the vaugnerites. The KCG can be explained by interactions between the CPG/MPG and the vaugnerites, or extensive differentiation of the latter. The new dataset provides clear evidence that the eastern FMC was affected by a long-lived magmatic episode characterized by coeval melting of both crustal and mantle sources. This feature is suggested here to result from

✉ Oscar Laurent
   oscarlaurent86@gmail.com

1 Institut für Geowissenschaften, J.W. Goethe Universität, Altenhöferallee 1, 60438 Frankfurt Am Main, Germany

2 Département de Géologie B20, Université de Liège, Quartier Agora, Allée du six Août 12, 4000 Liège, Belgium

3 Département de Géologie, Université Jean Monnet, UMR6524-CNRS-IRD 23 rue du Dr. Paul Michelon, 42023 Saint-Étienne, France

4 Department of Earth Sciences, University of Stellenbosch, Private Bag X1, Matieland 7602, South Africa

5 Abteilung Mineralogie und Petrologie, Institut für Angewandte Geowissenschaften, Karlsruher Institut für Technologie, Campus Süd, Kaiserstrasse 12, 76131 Karlsruhe, Germany

6 Géosciences Environnement Toulouse, Université Paul Sabatier, Observatoire Midi-Pyrénées 14 avenue E. Belin, 31400 Toulouse, France

7 Université d'Orléans, ISTO, UMR 7327, 45071 Orléans, France

8 CNRS, ISTO, UMR 7327, 45071 Orléans, France

9 BRGM, ISTO, UMR 7327, BP 36009, 45060 Orléans, France

10 LGL, TPE UMR5276, Université Lyon 1, Lyon, France

11 Department of Earth Sciences, University of Geneva, Rue des Maraîchers 13, Geneva 1205, Switzerland

12 Present Address: Institute for Geochemistry and Petrology, ETH Zürich, Zurich, Switzerland

🖄 Springer

a lithospheric-scale thermal anomaly, triggered by the removal of the lithospheric mantle root. The spatial distribution of the dated samples points to a progressive southward delamination of the lithospheric mantle, perhaps in response to rollback following continental subduction, or to "retro-delamination" owing to the retreat of a south-verging subduction zone.

Introduction

Following crustal thickening, the final stages of continental collision, associated with lateral extension or orogenic collapse, are periods of intense magmatic activity characterized by emplacement of granitoids derived from both crustal and mantle sources (Liégeois et al. 1998; Bonin 2004; Clemens et al. 2009; Vanderhaeghe 2012; Laurent et al. 2014a). Granitoid magmas represent major heat and mass transfers from the lower to the upper crust, contributing to crustal differentiation, thermal maturation and ore deposits (Petford et al. 2000; Kemp and Hawkesworth 2003; Hou and Cook 2009). Voluminous layers of partially molten rocks at mid to lower crustal levels, as evidenced in modern orogens by geophysical investigations (Nelson et al. 1996; Schilling and Partzsch 2001), influence the thermo-mechanical behavior of the orogenic crust and its coupling to the lithospheric mantle (Brown 2001; Vanderhaeghe and Teyssier 2001; Schulmann et al. 2008; Vanderhaeghe 2009; Barbey et al. 2015). In addition, the mafic magmas emplaced during these periods and their derivatives may represent significant additions to the preexisting continental volume (Laurent et al. 2013; Couzinié et al. 2016; Moyen et al. in press). Therefore, late- to post-collisional magmatism is of primary interest to understand (i) the mechanisms of heat and mass transfer in the lithosphere; (ii) the geodynamic evolution at convergent plate boundaries; and (iii) continental crust formation and differentiation.

The Paleozoic Variscan belt of western Europe is often referred to as a "hot" orogen (Schulmann et al. 2008) characterized by the emplacement of abundant and diverse granitoid magmas, especially at the end of the continental collision sensu stricto and throughout late-orogenic collapse (Pin and Duthou 1990; Finger et al. 1997; Gardien et al. 1997; Fernández-Suárez et al. 2000; Janoušek et al. 2000; Rossi and Pin 2008). In the French Massif Central (FMC), the late-Variscan collapse led to the formation of the 305–300 Ma Velay granite–migmatite complex (Montel et al. 1992; Mougeot et al. 1997; Couzinié et al. 2014), a roughly circular dome of >100 km diameter and >6000 km^2 (Fig. 1), consisting of migmatites cored by a heterogeneous

cordierite-bearing granite (Ledru et al. 2001; Barbey et al. 2015). It is suggested that the Velay dome was formed in response to a long-lived (>40 Ma) period of HT metamorphism and partial melting of the orogenic crust (Vanderhaeghe et al. 1999; Ledru et al. 2001; Vanderhaeghe and Teyssier 2001; Rossi and Pin 2008), first through limited low-temperature, possibly water-present melting between ca. 340 and 314 Ma; and second through high-temperature, extensive biotite breakdown melting at 310–300 Ma (Montel et al. 1992; Mougeot et al. 1997; Barbey et al. 1999, 2015; Couzinié et al. 2014).

Field relationships indicate that voluminous granitoid plutons and batholiths were emplaced before, during and after its formation (Ledru et al. 2001; Faure et al. 2009). Indeed, available geochronological data hint that granite formation lasted for several tens of million years between the early Carboniferous (340 ± 20 Ma) and early Permian (295 ± 15 Ma) (Duthou et al. 1984; Montel et al. 1992; Briand et al. 2002; Bé Mézème et al. 2006; Table 1). Moreover, granitoids are associated with volumetrically minor, but spatially ubiquitous mafic magmas, i.e., potassic to ultrapotassic diorites, gabbros and/or lamprophyres, locally referred to as "vaugnerites" (Sabatier 1991; Solgadi et al. 2007; Scarrow et al. 2008; von Raumer et al. 2013; Couzinié et al. 2014, 2016). Several questions arise from those observations. First, the genesis of large volumes of granite throughout the Carboniferous apparently contradicts the model proposed by some authors for the formation of the Velay dome, which implies that crustal anatexis was limited prior to 310 Ma and only produced significant amounts of granitic magmas at 310–300 Ma (Montel et al. 1992; Ledru et al. 2001). It has also been proposed that the formation of these granites and their ascent through the crust explains the temperature increase associated with the formation of the Velay dome at 310–300 Ma (Barbey et al. 2015), but then the problem translates to the origin of the heat source responsible for the genesis of the granites (Rossi and Pin 2008). Second, the role played by mafic magmas in the late-orogenic evolution is poorly understood; in particular, it is not yet clear whether the mafic magmas are responsible for crustal melting, or whether they represent a side effect of the processes at the origin of crustal anatexis.

To be addressed, those problems require a reliable geochronological framework for both granitic and mafic magmatism. Such a dataset is still lacking in the eastern FMC, where most available ages are either imprecise and possibly inaccurate radiometric dates based on whole-rock isochrons (Rb–Sr or Sm–Nd) or recent U–Pb dates but focused on small areas or specific plutons. This prevents a large-scale and systematic understanding of the magmatic evolution and questions the existence of long-lived granitic emplacement prior to the formation of the Velay complex, since this may only be an artifact of the large uncertainties
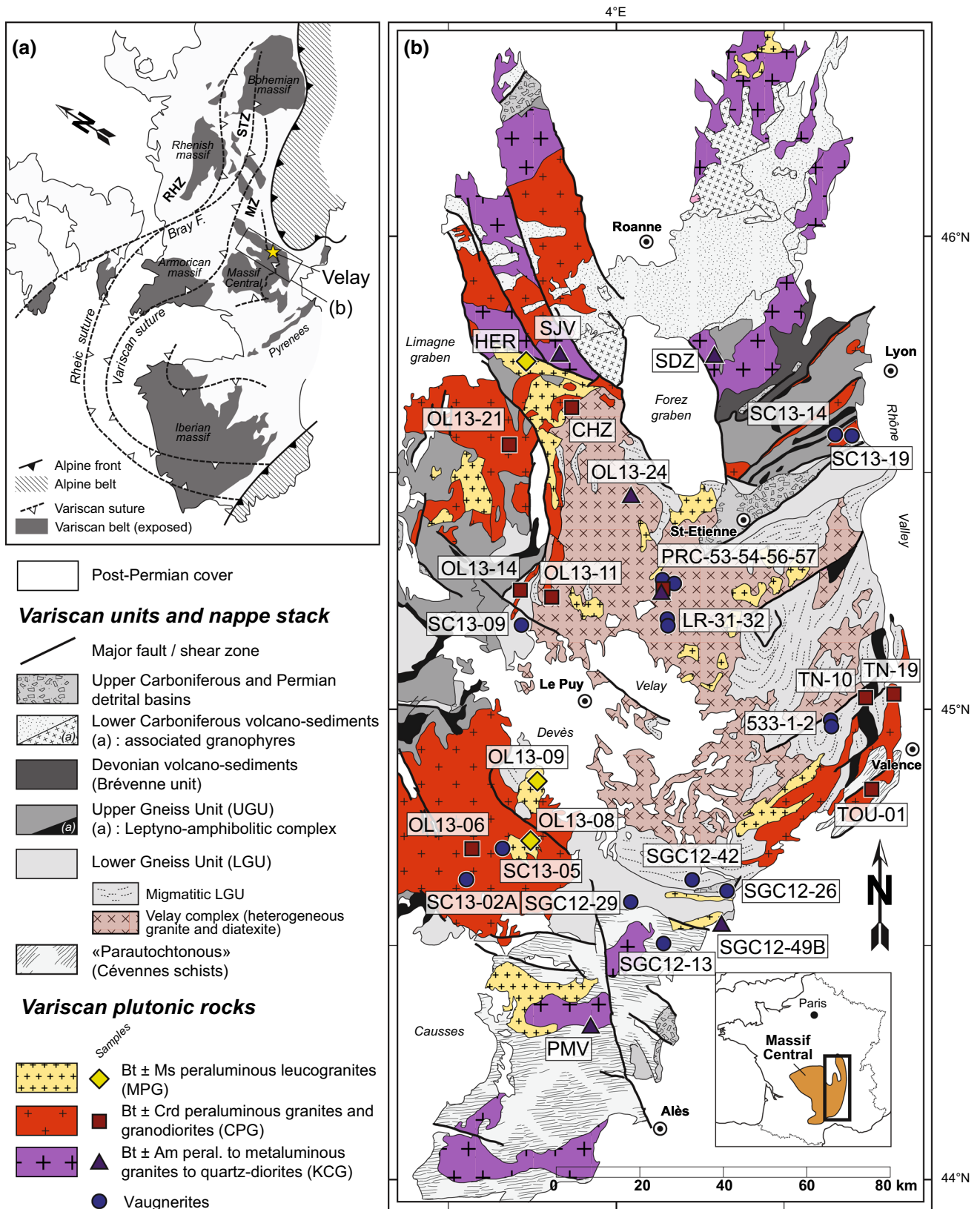
Fig. 1 **a** Sketch map showing the repartition of exposed Variscan domains in Western Europe, as well as the salient structural features of the Variscan belt (*MZ* moldanubian zone, *RHZ* Rheno-Hercynian zone, *STZ* Saxo-Thuringian zone). **b** Geological map of the eastern French Massif Central (after the 1:1000000^e BRGM map of France) with particular emphasis on the late-Variscan plutonic rocks associated with the Velay Complex. Positions of the studied samples are also indicated

Table 1 List, nature and sampling localities of the investigated samples of Variscan igneous plutonic rocks from the eastern FMC, together with existing age data and results of zircon and monazite U–Pb dating performed in this study

Sample	Nature	Type[a]	Pluton/locality	Encl.[b]	Lat. N	Long. E	Literature age (Ma)[c]	Ref.[d]	Method[d]	Group[e]	Age (Ma)[f]	±2σ	MSWD[g]	Prob[g]	C[h]	M[h]	I[h]	N[h]	Z[h]
CHZ	Porph. Bt granite	CPG	Chalmazel	y	45°42′15″	3°52′07″				3	**332.0**	**2.0**	0.58	0.87	7	17	5	22	19
HER	Bt-Ms leucogranite	MPG	Hermitage	n	45°45′50″	3°46′23″	329 ± 14	1	Rb/Sr WR	3	**325.7**	**1.3**	0.62	0.78	5	20	8	28	25
OL-13-06	Porph. Bt-Crd granite	CPG	Margeride	n	44°40′28″	3°26′01″	334 ± 9	2	U/Pb Zrn (TIMS)	2	**312.9**	**2.0**	0.39	0.98	8	33	–	33	28
							323 ± 12	3	Rb/Sr WR										
							314 ± 4	4	U/Pb Mnz (TIMS)										
OL-13-08	Bt-Ms leucogranite	MPG	Grandrieu	n	44°43′42″	3°40′26″	305 ± 4	5	U/Pb Mnz (TIMS)	3	**311.0**	**1.1**	1.12	0.34	6	13	25	38	35
											309.3[i]	1.2	1.10	0.36	6				
OL-13-09	Bt-Ms leucogranite	MPG	St-Christophe-d'Allier	n	44°49′07″	3°42′43″	305 ± 14	6	U/Pb Mnz (TIMS)	3	**312.7**	**2.3**	0.61	0.82	6	6	19	25	19
OL-13-11	Bt granite	CPG	Almance	n	45°18′16″	3°46′44″				3	**314.5**	**1.7**	0.25	0.99	5	15	15	30	28
											315.4[i]	0.9	0.86	0.60	8				
OL-13-14	Porph. Bt-Crd granite	CPG	Chaise-Dieu	n	45°19′37″	3°41′20″				3	**318.3**	**2.6**	0.44	0.88	4	18	31	49	39
											317.8[i]	1.3	1.60	0.10	5				
OL-13-21	Bt granite	CPG	St-Dier-d'Auvergne	n	45°40′18″	3°38′45″	330 ± 26	7	Rb/Sr WR	3	**336.9**	**1.8**	0.99	0.47	11	19	7	26	26
OL-13-24	Bt-Am Qz-diorite	KCG	Gumières	y	45°31′48″	3°59′09″	313 ± 2	8	U/Pb Zrn (LA)	1	**321.2**	**1.2**	1.40	0.03	27	32	–	32	30
PMV	Porph. Bt-Am granite	KCG	Pont-de-Montvert	n	44°20′06″	3°52′30″				2	**302.5**	**0.9**	1.06	0.38	13	24	2	26	24
PRC-56	Bt-Am granodiorite	KCG	Pont-Rouge quarry	y	45°19′44″	4°06′08″				1	**332.1**	**0.7**	1.40	0.03	26	31	–	31	30
PRC-57	Bt-Crd granite	CPG	Pont-Rouge quarry	n	45°19′44″	4°06′08″	305.9 ± 1.4	9	U/Pb Mnz (LA)	3	**302.8[i]**	**1.3**	1.50	0.09	10	11	21	32	32
											334.9[i]	1.5	1.50	0.10	7				
SDZ	Bt granite	KCG	Salt-en-Donzy	n	45°47′02″	4°18′25″				2	**337.4**	**1.0**	1.50	0.03	16	29	2	31	23

Table 1 continued

Sample	Nature	Type[a]	Pluton/locality	Encl.[b]	Lat. N	Long. E	Literature age (Ma)[c]	Ref.[d]	Method[d]	Group[e]	Age (Ma)[f]	±2σ	MSWD[g]	Prob[g]	C[h]	M[h]	I[h]	N[h]	Z[h]
SGC-12-49B	Porph. Bt-granite	KCG	Largentière	n	44°33′17″	4°17′15″	304.1 ± 6.3	9	U/Pb Zrn (LA)	2	298.9	1.8	0.61	0.90	10	18	2	20	18
SJV	Bt-Am granodiorite	KCG	St-Julien-la-Vêtre	n	45°48′32″	3°50′07″	340 ± 20	10	Rb/Sr WR	2	330.1	1.3	1.11	0.28	14	28	–	28	26
TN-10	Poph. Bt-granodiorite	CPG	Colombier-le-Vieux	y	45°03′31″	4°43′57″				3	321.9	1.3	1.60	0.11	5	27	7	34	30
TN-19	Porph. Bt granite	CPG	Tournon	n	45°04′10″	4°49′35″	337 ± 13	11	Rb/Sr WR	3	321.1	1.1	1.17	0.07	6	14	17	31	31
TOU-01	Porph. Bt granite	CPG	Dunières-sur-Eyrieux	n	44°49′45″	4°39′08″				3	322.2	1.5	0.47	0.98	10	22	8	30	24
533-1	Vaugnerite		Lamastre	n	44°58′24″	4°37′41″				1	307.8	1.6	1.05	0.40	12	16	–	16	5
533-2	Vaugnerite		Lamastre	n	44°58′24″	4°37′41″				2	307.3	1.3	0.73	0.87	18	27	–	27	26
LR-31	Vaugnerite		La Roche	n	45°17′05″	4°06′50″				1	299.1	1.3	0.75	0.85	17	20	–	20	20
LR-32	Vaugnerite		La Roche	n	45°17′05″	4°06′50″				1	301.5	1.4	0.71	0.88	17	19	–	19	17
PRC-53	Vaugnerite		Pont-Rouge quarry	y	45°19′47″	4°06′05″				2	318.9	1.8	0.48	0.98	11	22	–	22	22
PRC-54	Vaugnerite		Pont-Rouge quarry	y	45°19′47″	4°06′05″				2	320.5	1.8	0.42	0.99	11	17	–	17	17
SC-13-02A	Vaugnerite		Moulin de Linas	n	44°41′14″	3°28′25″				1	313.2	2.5	0.53	0.85	5	7	–	7	5
SC-13-05	Vaugnerite		L'Aldeyres	n	44°45′53″	3°37′53″				2	309.4	1.5	1.40	0.09	12	18	–	18	17
SC-13-09	Vaugnerite		Pubellier	n	45°13′29″	3°39′33″				1	309.7	1.2	1.19	0.19	21	26	1	27	27
SC-13-14	Vaugnerite		Marcenod	n	45°35′04″	4°29′32″				2	335.7	2.1	0.34	0.99	9	18	4	22	20
SC-13-19	Vaugnerite		Chassagny	n	45°36′14″	4°42′60″				1	333.9	1.4	0.92	0.60	17	26	–	26	24
SGC-12-13	Vaugnerite		Borne	n	44°29′48″	4°05′19″				1	306.6	2.4	0.59	0.84	6	9	–	9	8
SGC-12-26	Vaugnerite		Pont-de-Bayzan	n	44°39′28″	4°18′24″				1	306.1	1.3	1.04	0.39	20	24	–	24	24

Table 1 continued

Sample	Nature	Type[a]	Pluton/locality	Encl.[b]	Lat. N	Long. E	Literature age (Ma)[c]	Ref.[d]	Method[d]	Group[e]	Age (Ma)[f]	±2σ	MSWD[g]	Prob[g]	C[h]	M[h]	I[h]	N[h]	Z[h]
SGC-12-39	Vaugnerite		Loubaresse	n	44°36′02″	4°04′14″	307.4 ± 1.8	9	U/Pb Zrn (LA)	1	**306.6**	**1.6**	0.66	0.88	12	14	–	14	14
							313 ± 3	12	U/Pb Zrn (TIMS)										
SGC-12-42	Vaugnerite		Meyras	n	44°40′21″	4°16′26″	305.8 ± 2.3	9	U/Pb Zrn (LA)	1	**305.9**	**1.7**	0.56	0.95	11	16	–	16	16
							314 ± 3	12	U/Pb Zrn (TIMS)										

[a] For granitoids, classification according to Barbarin (1999)

[b] Occurrence as enclave in the Velay granite (yes/no)

[c] Existing age for the corresponding pluton or magmatic body

[d] Reference, dating system and technique for the age displayed in (c). 1 = Pin and Barbarin (unpublished); 2 = Respaut (1984); 3 = Couturié and Caen-Vachette (1979); 4 = Pin (1979b); 5 = Lafon and Respaut (1988); 6 = Isnard (1996); 7 = Saint-Joanis (1975); 8 = Barbarin et al. (2012); 9 = Couzinié et al. (2014); 10 = Pin (unpublished); 11 = Batias and Duthou (1979); 12 = Aït Malek (1997). *WR* whole-rock isochron, *Zrn* zircon, *Mnz* monazite, *LA* LA-ICP-MS

[e] Classification of the samples according to the distribution of U–Pb dates and zircon textures (see text for details)

[f] U–Pb Concordia age obtained in the course of this study, in Ma

[g] MSWD and Probability of concordance + equivalence for the displayed Concordia age

[h] C = number of analyses used to calculate the Concordia age; M = number of analyses corresponding to the "magmatic" age; I = number of analyses corresponding to zircon inheritance; N = total number of analyses for this sample (=$M + I$); Z = number of zircon grains analyzed in this sample (all for zircon data only)

[i] U–Pb Concordia age on monazite

[j] U–Pb Concordia age provided by zircons in sample PRC-57, probably reflecting inheritance (see "Discussion")

on the existing ages. In fact, the most recent U–Pb ages obtained on igneous rocks in the eastern FMC are almost exclusively in the range 310–300 Ma (Brichau et al. 2008; François 2009; Gardien et al. 2011; Barbarin et al. 2012; Didier et al. 2013; Couzinié et al. 2014), i.e., coeval with the migmatites and granites of the Velay dome. Furthermore, only a handful of ages are available so far on the mafic rocks (Aït-Malek 1997; Couzinié et al. 2014).

The aim of this study is therefore to provide a self-consistent geochronological dataset on both granites and mafic rocks in the eastern FMC. For this purpose, we sampled a total of 18 granitoids and 15 vaugnerites, representative of the lithological diversity observed at the regional scale, and performed U–Pb dating on individual zircons (and monazites for some samples) by laser ablation, sector field inductively coupled plasma mass spectrometry (LA-SF-ICP-MS). The results are used to discuss (i) the petrogenesis of the magmas; (ii) the nature of the heat source at the origin of late-Variscan magmatism in the eastern FMC; and (iii) its significance for the geological and tectonic evolution of the orogen.

Geological setting

The French Massif Central (FMC)

The Variscan belt of Western Europe (Fig. 1a) belongs to a Paleozoic orogenic system that results from convergence between Laurussia, Gondwana and several intervening microcontinents (Matte 1986; Kroner and Romer 2013; Stampfli et al. 2013), which ended up with the assembly of Pangea. The FMC is part of the inner domain of this belt (Lardeaux et al. 2014), referred to as the "Moldanubian" zone, and represents a reworked crustal domain that was previously formed along the northern margin of Gondwana (Faure et al. 2009; Melleton et al. 2010).

The FMC hosts a south-verging Devonian to early Carboniferous nappe pile (Ledru et al. 1989; Faure et al. 2009) that became dismembered by late Carboniferous ductile and brittle strike-slip shear zones and detachments accommodating late-orogenic extension and collapse (Malavieille et al. 1990; Faure 1995; Gardien et al. 1997). In the eastern FMC (Fig. 1b), this pile is made up from top to bottom (north to south) by:

1. The Brévenne unit, a greenschist-facies volcano-sedimentary basin (Feybesse et al. 1988) of late Devonian age (366 ± 5 Ma; Pin and Paquette 1997), presumably a back-arc system formed as a result of the southwards subduction of the Rheic Ocean (Lardeaux et al. 2014).
2. The Upper Gneiss Unit (UGU) consists of high-grade, migmatitic ortho- and paragneisses whose protoliths are early Ordovician in age (Duthou et al. 1984; Melleton et al. 2010; Chelle-Michou et al. 2015; Lotout et al. in press). The base of the UGU is characterized by the presence of (i) the leptynite–amphibolite complex (LAC), a bimodal Ordovician (487–478 Ma) magmatic association (Pin and Lancelot 1982; Briand et al. 1991) proposed to represent an ocean–continent transition zone (Lardeaux et al. 2014); and (ii) relics of (U)HP metamorphic rocks (Gardien et al. 1990; Mercier et al. 1991; Gardien 1993; Lardeaux et al. 2001).
3. The Lower Gneiss Unit (LGU) also made up of migmatitic ortho- and paragneisses with dominantly late Ediacaran to early Cambrian protolith age (Caen-Vachette 1979; Duthou et al. 1984; R'Kha Chaham et al. 1990; Couzinié et al. 2014; Chelle-Michou et al. 2015; Mintrone 2015) and minor amphibolites. The migmatites are cored by the heterogeneous Velay granite (Dupraz and Didier 1988; Ledru et al. 2001).
4. The Para-autochthonous Unit (PAU), dominantly made up of greenschist- to lower amphibolite-facies metasediments (Cévennes schists; Faure et al. 1999) deposited between the Neoproterozoic and the early Cambrian (Caron 1994; Melleton et al. 2010).

The tectono-metamorphic evolution of the eastern FMC can be summarized as follows. An early (D–M$_0$) (U)HP metamorphic event attributed to northward subduction was dated between 432 and 408 Ma (Pin and Lancelot 1982; Ducrot et al. 1983; Paquette et al. 1995; Do Couto et al. 2015) and recorded by the eclogitic relics (at the base of the UGU and in the LAC). The UGU experienced anatexis (M$_1$) coeval with exhumation of the (U)HP units and top-to-the-SW shearing (D$_1$) (Faure et al. 2008, 2009) between 384 ± 16 Ma (Duthou et al. 1994) and 360 ± 4 Ma (Gardien et al. 2011). The UGU was subsequently juxtaposed to the north to the Brévenne unit during top-to-the-NW (D–M$_2$) thrusting (Leloix et al. 1999) at ~360–350 Ma (Faure et al. 2002). This episode is also recorded in the western part of the FMC (Limousin area) by 360 ± 4 Ma top-to-the-NW thrusting (Melleton et al. 2009) and corresponds to the main event of nappe stacking (Faure et al. 2009). The early Carboniferous D$_3$ event corresponds to the onset of syn-orogenic extension in the northern part of the FMC, as recorded by 340–330-Ma-old volcano-sedimentary sequences (Bruguier et al. 1998), while crustal thickening was still ongoing in the southern domain, especially the PAU which experienced top-to-the-S thrusting (Arnaud and Burg 1993; Caron 1994). Subsequently, the nappe pile, specifically the LGU, was extensively reworked by a pervasive Carboniferous LP–HT event that culminated with the rise of the Velay dome (Ledru et al. 2001). This reworking process was proposed to happen in two steps (Montel et al. 1992; Barbey et al. 2015): (i) limited anatexis in the LGU with biotite remaining stable
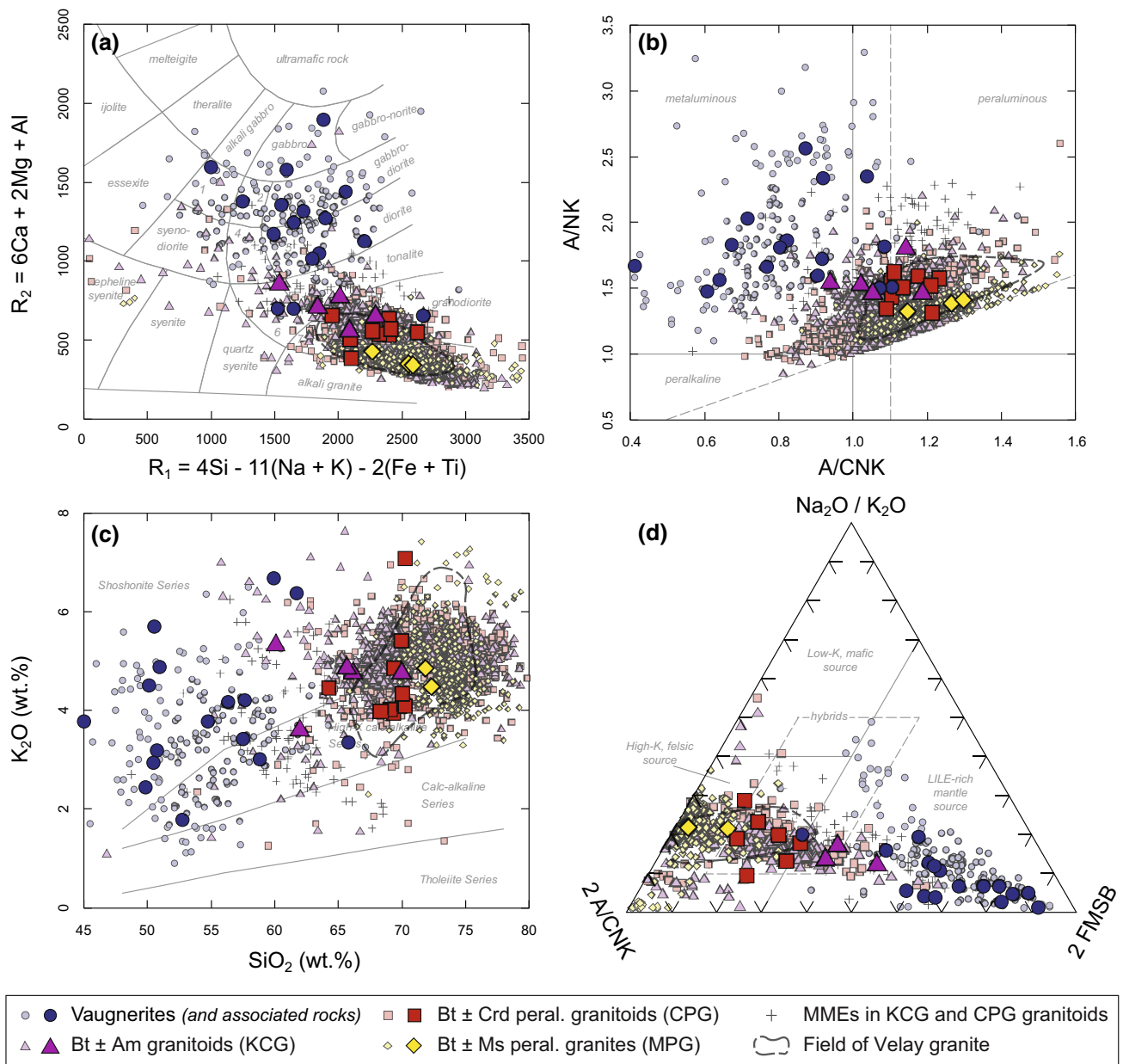
Fig. 2 Some geochemical characteristics of late-Variscan plutonic rocks in the eastern French Massif Central. The larger symbols correspond to samples investigated in the present study for which whole-rock geochemical data are available (unpublished data from S. Couzinié). **a** R_1–R_2 plot of De la Roche et al. (1980) (1 = syenogabbro; 2 = monzogabbro; 3 = monzonite; 4 = monzodiorite; 5 = quartz–monzonite; 6 = granite); **b** molar $Al_2O_3/(Na_2O + K_2O)$ (A/NK) vs. $Al_2O_3/(CaO + Na_2O + K_2O)$ (A/CNK) plot; **c** K_2O vs. SiO_2 plot (fields are from Peccerillo and Taylor 1976); and **d** ternary discrimination plot of Laurent et al. (2014a, b) proposed on the basis of late-Archean granitoid typology (FMSB = [FeOt + MgO]$_{wt\%}$ × [Sr + Ba]$_{wt\%}$)

($T < 750$ °C), at ages between 329 ± 5 Ma (Bé Mézème et al. 2006) and 314 ± 5 Ma (Mougeot et al. 1997); and (ii) widespread biotite dehydration melting ($760 < T < 850$ °C) that affected the whole middle crust and gave rise to the formation of the Velay dome proper at 301–305 Ma (Couzinié et al. 2014). Those late Carboniferous events are attributed to N(W)–S(E)-directed late-orogenic extension ($D_{4–5}$) associated with large-scale crustal detachments and formation of

detrital coal-bearing basins (Malavieille et al. 1990; Faure et al. 2009).

## Petrographic-geochemical characteristics of late-Variscan igneous rocks in the eastern FMC

Exposure in the eastern FMC is largely dominated by Carboniferous plutonic rocks intruding the metamorphic

lithologies described earlier (Fig. 1b). Based on existing petrographic descriptions and classifications (Didier and Lameyre 1969; Didier et al. 1982; Barbarin 1983, 1992, 1999; Stussi and De la Roche 1984; Rossi and Pin 2008; Moyen et al. in press), four types of plutonic rocks can be distinguished (Fig. 1b) (nomenclature after Barbarin 1999):

1. Peraluminous to slightly metaluminous, biotite- and sometimes cordierite-bearing granitoids ("**CPG**") are the most abundant (Fig. 1b). They can be separated in two subgroups: (i) K-feldspar porphyritic, cordierite-poor plutons and batholiths (Margeride, Chaise-Dieu, Tournon) characterized by the presence of microgranular mafic enclaves (MMEs; Didier et al. 1982) and (ii) the cordierite-rich, heterogeneous Velay granite, which is closely associated with LGU migmatites and fre-

quently contains large enclaves of the previous, cordierite-poorer type (Barbey et al. 2015; Ledru et al. 2001; Williamson et al. 1997). CPG are granites and granodiorites (Fig. 2a) with a peraluminous character (Fig. 2b) and elevated contents in SiO_2 (>65 wt%) and K_2O (3–7 wt%) (Fig. 2c). Those characteristics, together with Sr–Nd isotopic data, reflect that the CPG result from partial melting of the local crust (Duthou et al. 1984; Pin and Duthou 1990; Downes et al. 1997; Williamson et al. 1997).

2. Peraluminous, two-mica or muscovite-bearing (leuco-) granites ("**MPG**"), generally occurring as dykes and small laccoliths intrusive in the Velay complex (Ledru et al. 2001; Didier et al. 2013) as well as rare plutons (L'Hermitage, Saint-Christophe-d'Allier). The MPG show a tighter compositional range than the CPG. They
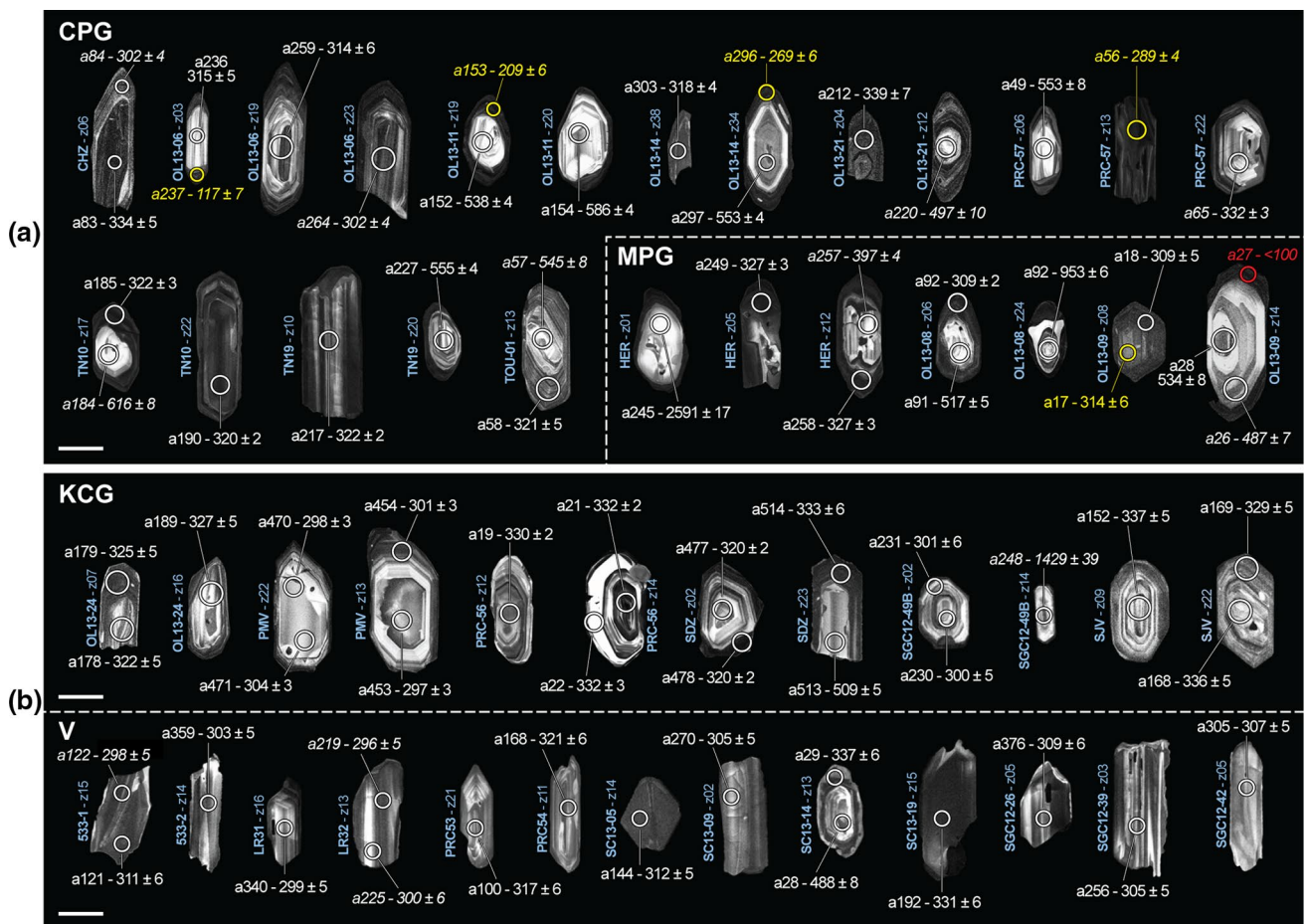
Fig. 3 Representative cathodoluminescence images of zircon grains from samples of late-Variscan plutonics rocks investigated in this study: **a** cordierite- and muscovite-bearing peraluminous granites (CPG and MPG); **b** K-feldspar porphyritic calc-alkaline granites and granodiorites (KCG) and vaugnerites (V). The position of the laser spots used for U–Pb dating (*circles*) is also indicated, along with the spot name (aXXX) and the corresponding $^{238}U/^{206}Pb$ age (with $\pm2\sigma$ uncertainty, in Ma). Each zircon grain is labeled with the sample it was extracted from and its number in this sample (zXX). Values with an *asterisk* indicate $^{207}Pb/^{206}Pb$ ages; labels in italics indicate >5% discordance. The *yellow circles* and font highlight analyses with large amounts of common ^{204}Pb (>5%); the *red circle* and font indicate an analysis (a27) from which no reliable age could be obtained because of high discordance and common Pb contents, and that was therefore discarded. The *scale bar* is 100 μm

are granites sensu stricto (Fig. 2a) with a clearer peraluminous character (Fig. 2b) and restricted to SiO_2 contents >70 wt% (Fig. 2b–c), pointing to a crustal source (Pin and Duthou 1990; Barbarin 1999) (Fig. 2d).

3. Weakly peraluminous to metaluminous, K-feldspar porphyritic, biotite- ± amphibole-bearing granites, granodiorites and quartz–diorites ("**KCG**"). They either form large plutons (Saint-Julien-la-Vêtre, Pont-de-Montvert, Aigoual) or enclaves within the Velay complex, of various sizes (a few cm across to pluri-kilometric screens like the Gumières enclave; Barbarin et al. 2012). The composition of the KCG largely overlaps that of the CPG, yet they are on average slightly more "mafic" than the latter (average SiO_2 and FeO_t + MgO of KCG are ~69 and ~4.0 wt%, respectively, against ~72 and ~2.5 wt% for CPG) (Fig. 2). This makes KCG chemically intermediate between vaugnerites and MPG–CPG (Fig. 2) and led several authors to propose that they result from magma mixing between vaugnerites and crustal melts (Downes et al. 1997; Solgadi et al. 2007).

4. A suite of metaluminous, biotite-, amphibole- ± clinopyroxene-bearing intermediate to mafic rocks locally called "**vaugnerites**", which are akin to Mg–K magmatic rocks such as appinites, durbachites and lamprophyres (Sabatier 1991; Rossi and Pin 2008; Scarrow et al. 2008; von Raumer et al. 2013; Couzinié et al. 2014, 2016). Although they do not form mappable bodies at the scale of Fig. 1b, they are regionally ubiquitous and occur as enclaves (0.1–100 m in size) in the granitoids (Didier et al. 1982; Ledru et al. 2001), kilometric stocks and lamprophyric dykes. They form a compositionally heterogeneous group of gabbroic to dioritic rocks (Fig. 2a), yet all characterized by metaluminous affinities (Fig. 2b), lower SiO_2 (45–65 wt%) and higher FeO_t + MgO (up to 25 wt%) than coexisting granitoids, together with high-K to shoshonitic affinities (K_2O = 1.5–6.0 wt%) and richness in incompatible trace elements (Sr + Ba, but also REE and HFSE) (Fig. 2c, d). This dual geochemical character clearly points to an enriched (metasomatized) lithospheric mantle source (Sabatier 1991; Solgadi et al. 2007; von Raumer et al. 2013; Couzinié et al. 2014, 2016).

Analytical methods

We selected 33 samples for U–Pb dating, collected throughout the eastern MCF (Fig. 1b) and representative of the geochemical diversity reported earlier (Table 1; Fig. 1b). Samples weighing 5–10 kg were reduced using jaw and disk mills and sieved to <500 μm. Heavy minerals were extracted by using conventional concentration techniques (shaking table, magnetic separator, heavy liquids). Between 50 and 100 zircon grains per sample, but also monazite wherever available, were handpicked, set in 1-inch epoxy mounts and polished to expose their interiors. The internal structures of these grains were characterized by cathodoluminescence (CL) and back-scattered electron (BSE) imaging prior to LA-SF-ICP-MS dating using (i) a Jeol JSM-6490 scanning electron microscope (SEM) equipped with a Gatan MiniCL at Goethe University Frankfurt (GUF) for the granite samples and (ii) a ZEISS EVO-150 SEM at University of Granada (Spain) for the vaugnerite samples.

U–Pb isotopic analyses were carried out at GUF by laser ablation using a Resolution M-50 (Resonetics) 193-nm ArF excimer laser system attached to Thermo Finnigan Element 2 sector field ICP-MS. A detailed description of the analytical techniques is available in the Supplementary Material. The data were corrected offline for background signal, common Pb, instrumental mass discrimination and downhole Pb/U fractionation using an in-house MS Excel© spreadsheet (Gerdes and Zeh 2006, 2009). For both zircon and monazite analyses, the corrections and determination of U, Th and Pb compositions were performed using normalization to standard zircon GJ-1. Reference materials Plešovice, OG-1 and BB (for zircon sessions) and Moacir, Manangoutry and in-house WM (for monazite sessions) were used as secondary standards to check the accuracy of the corrections, and all provide ages in good agreement with the reference values (see supplementary material Table S1). Age calculations and data plotting were performed using the Isoplot toolkit (Ludwig 2008) v.4.15 for MS Excel©. The complete dataset is available as supplementary material (Table S2).

Results

Zircon textures

Figure 3 shows representative CL and BSE images of zircons from igneous plutonic rocks of the eastern FMC. Zircon characteristics depend on the rock type considered. The MPG and CPG show heterogeneous zircon populations, having a range of sizes (from 50 up to 500 μm) and shapes (aspect ratios between 1.5 and 8), some of them being obvious xenocrysts (broken or irregular edges crosscutting the internal zoning). Grains with clear core–rim relationships are very common in both granitoid types: they show rounded or sub-idiomorphic CL-bright cores with oscillatory zoning, wrapped by CL-darker rims (Fig. 3a). The rims often show irregular or very fine oscillatory zoning, occasionally with porous textures and/or inclusions, and are generally wider (>50 μm) in CPG than in MPG (<50 μm) (Fig. 3a). The CPG and MPG also contain core-free,
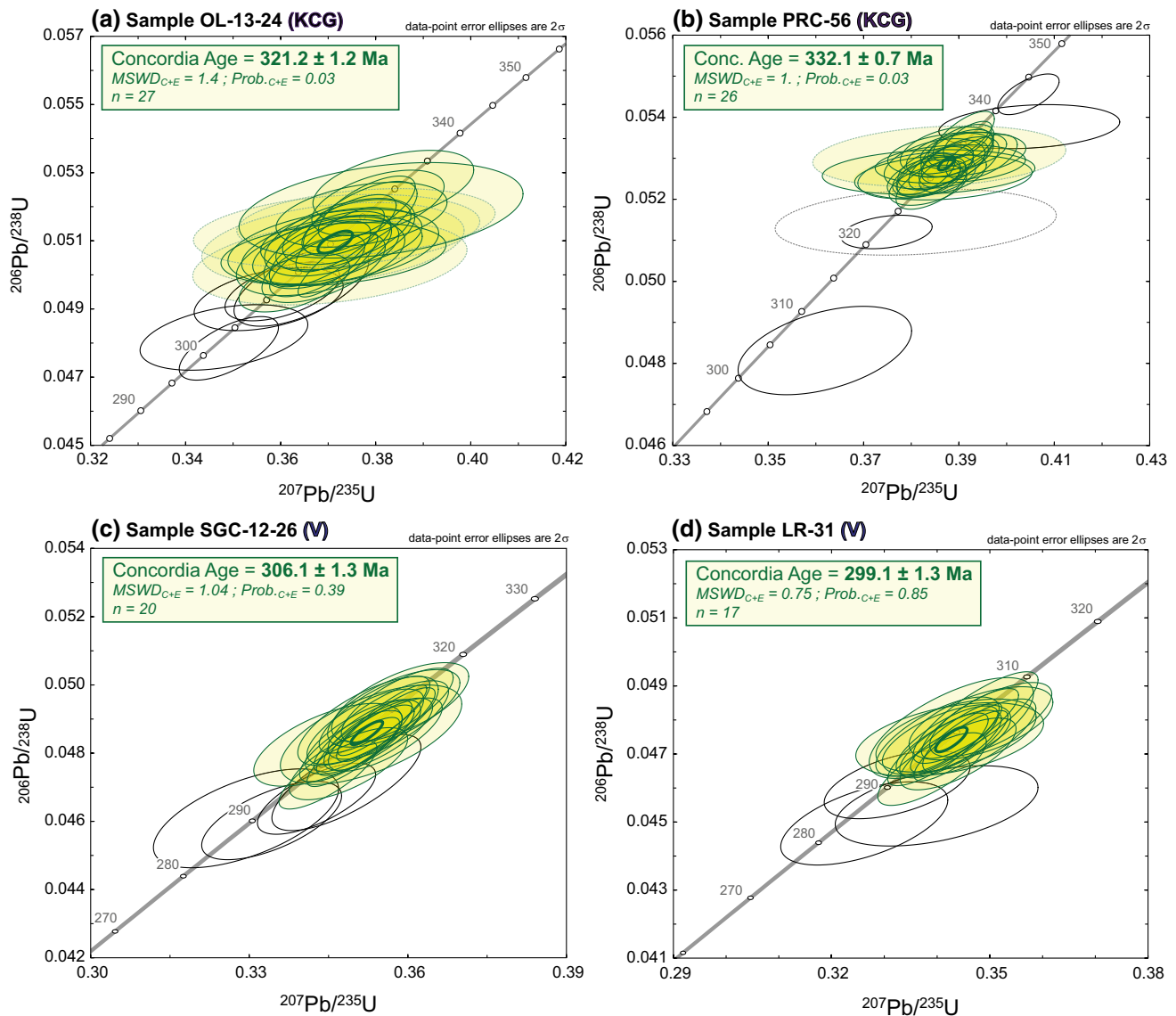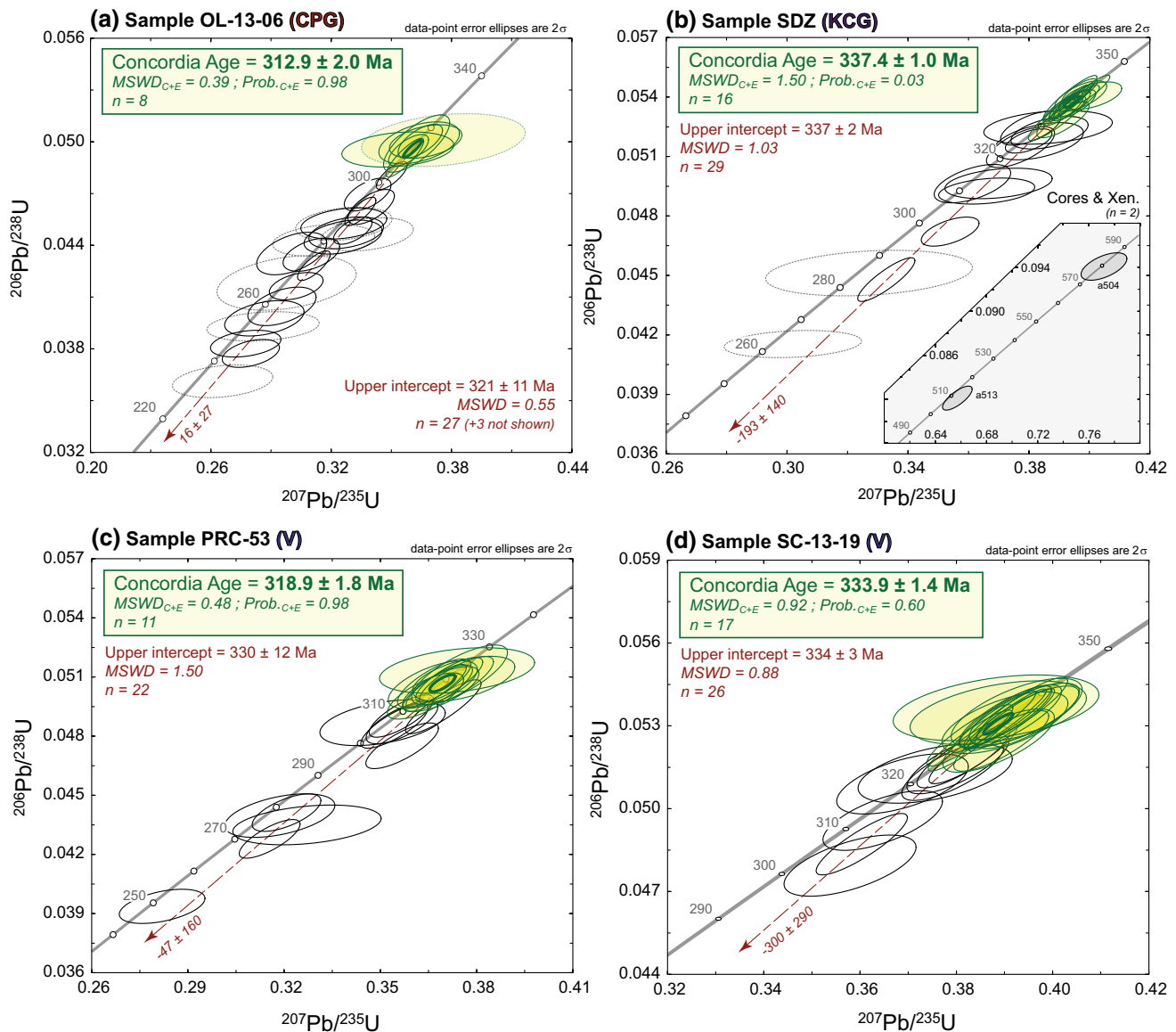
Fig. 4 Representative U–Pb Concordia diagrams (^{206}Pb/^{238}U vs. ^{207}Pb/^{235}U) showing examples of zircon analyses from samples of "group 1" (V = vaugnerite), i.e., showing a single generation of zircon dates with mostly identical ^{206}Pb/^{238}U ratios within uncertainties (see "Discussion"). Green ellipses are the oldest, equivalent concord-

ant analyses from zircon rims or crystals devoid of any core (excluding outliers), used for the calculation of the Concordia Age. The *dashed ellipses* represent analyses with >5% of common ^{204}Pb. All ages are quoted to 2σ level of uncertainty

idiomorphic to xenomorphic crystals (scarce in MPG but dominant in CPG). These are relatively CL-dark, and show irregular or banded zoning patterns (Fig. 3a). A notable exception among the CPG is sample OL-13-06 (Margeride granite), of which zircons are relatively CL-bright, and display a well-developed oscillatory zoning and distinct aspect ratios (Fig. 3a).

Zircon grains in the KCGs are less diverse than in the CPG and MPG, and seldom show core–rim relationships (if any). Resorbed cores occasionally occur in samples SDZ (Fig. 3b) and PMV, and a single xenocryst was found in sample SGC-12-49B (Fig. 3b). The crystals are usually

100–350 μm long, form idiomorphic prisms with aspect ratios between 1.5 and 3, and reveal a concentric oscillatory zoning. They are CL-brighter than the zircons from the CPG and MPG (Fig. 3b). Zircon populations in vaugnerites are very homogeneous within a given sample, without any core–rim relationships (except sample SC13-14; Fig. 3b). The crystals range in size from 70 to 500 μm and display various shapes, from short prismatic to needle-shaped (aspect ratios between 1.5 and 6). In most samples, the grains appear CL-dark and display striped or sector zoning, but in two SiO$_2$-richer samples (quartz–syenites PRC-53 and PRC-54), oscillatory zoning is predominant (Fig. 3b).

Fig. 5 Representative U–Pb Concordia diagrams (^{206}Pb/^{238}U vs. ^{207}Pb/^{235}U) showing examples of zircon analyses from samples of "group 2" (V = vaugnerite), i.e., showing a single generation of zircon (i.e., scarce or no core–rim relationships) but scattered ^{206}Pb/^{238}U dates with a Carboniferous upper intercept age, and a lower intercept at or close to zero within uncertainty. The *inset* in the bottom right of **b** represents a close-up to the analyses from two zircon cores, reported as shaded ellipses. *Green ellipses* are the oldest, equivalent concordant analyses from zircon rims or crystals devoid of any core (excluding outliers), used for the calculation of the Concordia Age. The *dashed ellipses* represent analyses with >5% of common ^{204}Pb. The *dashed red lines* are regressions through all the data from zircon rims or crystals devoid of any core; the arrow and numbers in italics point to the lower intercept. All ages are quoted to 2σ level of uncertainty

Back-scattered electron (BSE) images of monazite grains from the four samples in which this mineral was investigated are reported in the Supplementary Material.

U–Pb dates

Zircon populations were dated in 33 samples and monazite grains in four of them (OL-13-08, OL-13-11, OL-13-14, PRC-57). A detailed description of the data, statistics, as well as the complete set of Concordia diagrams, is available in the Supplementary Material. The most important points arising from this description, together with representative Concordia diagrams, are reported hereafter.

Based on the combination of U–Pb dating results and zircon textures, the investigated samples can be subdivided into three major groups (Table 1):

- *Group 1* (Fig. 4) samples are characterized by (i) zircons with the absence of any core–rim relationship; and (ii) zircon U–Pb analyses yielding a single generation of Carboniferous (to early Permian) U–Pb dates, the majority of which (>65% and commonly up to 85%) being identical within uncertainties and concordant. This includes most vaugnerite samples as well as two KCG (OL-13-24 and PRC-56).
- *Group 2* (Fig. 5) includes samples containing very few or no zircon cores, and a dominant population of zircons showing scattered $^{206}Pb/^{238}U$ dates younger than 340 Ma, specifically defining trends with a Carboniferous upper intercept and a lower intercept at or around zero within uncertainty. This group comprises most KCG samples, a few vaugnerites and one single CPG sample (OL-13-06).
- *Group 3* (Fig. 6) samples are characterized by two clear populations of zircon textures and dates, roughly equivalent regarding the number of analyses: (i) abundant zircon cores with U–Pb dates ranging from early Carboniferous (~340 Ma) to late-Archean (~2600 Ma) (those problems require a reliable geochronological 98; 42%) and (ii) zircon rims or grains devoid of any core, having U–Pb data repartition similar to that observed for group 2 samples, i.e., scattered U–Pb dates defining a Carboniferous upper intercept and a lower intercept close to zero ($n = 134$; 58%). This group encompasses all MPG and CPG samples, except sample OL-13-06.

Figure 7 compiles the data obtained from zircon cores in samples of groups 2 and 3. Out of 170 analyses, 106 are >90% concordant, with only few of them having dates >800 Ma ($n = 12$). The others reveal a nearly continuous date spectrum between 740 and 340 Ma, with a major peak at 540 ± 20 Ma ($n = 45$; 42% of all concordant data), and minor peaks at 475 ± 20 Ma ($n = 12$); 625 ± 10 Ma ($n = 6$); 375 ± 10 Ma ($n = 8$); and 340 ± 10 Ma ($n = 5$). There are additional minor peaks at 850 ± 15 Ma ($n = 3$) and ~955 Ma ($n = 2$), and a few grains reveal (mostly discordant) dates between ~1025 and ~2600 Ma.
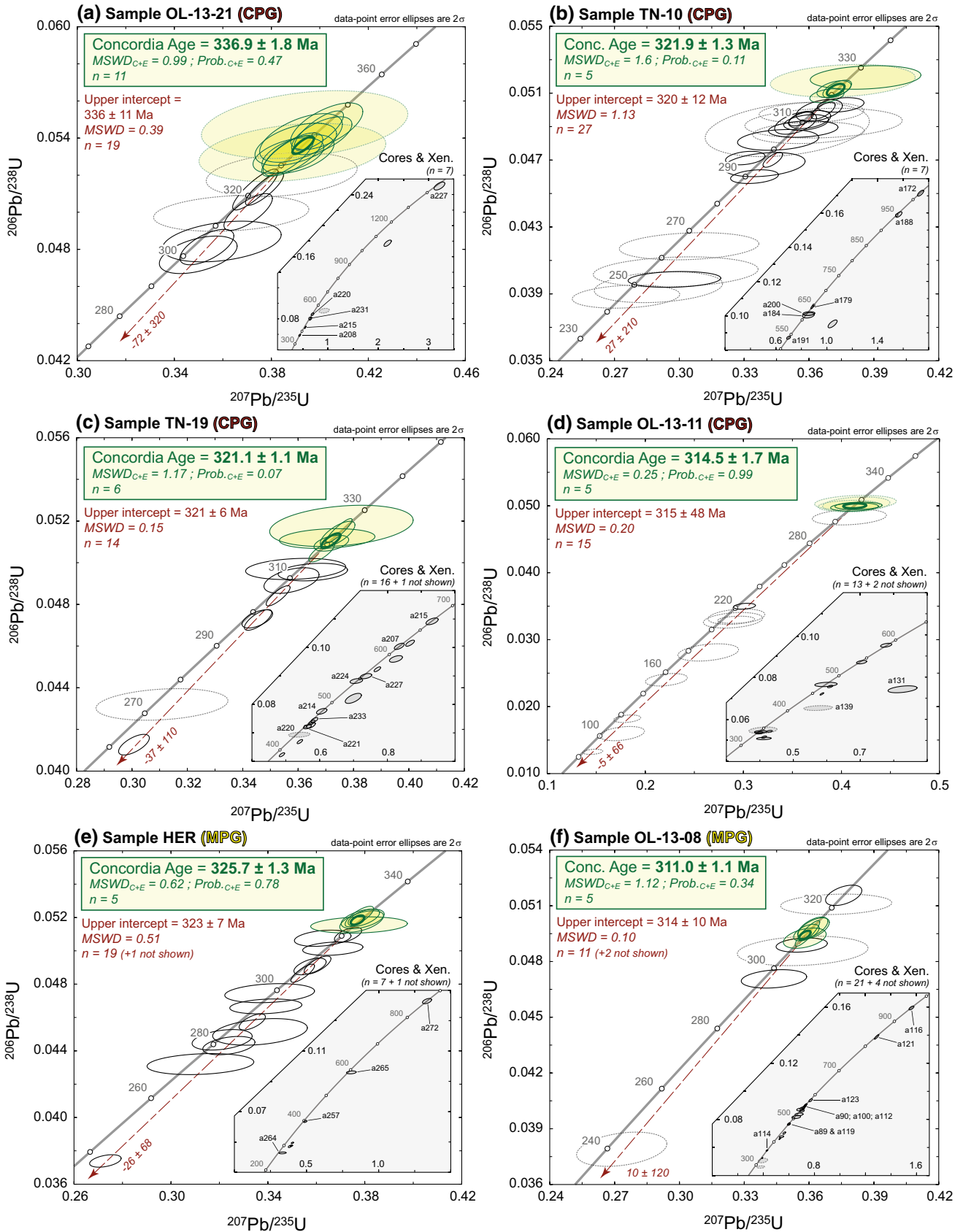
Discussion

From date to age: interpretation of U–Pb data

In the following, the signification of zircon U–Pb dates obtained in each group of samples presented in the previous section is discussed, on the basis of zircon textures and U–Pb data. These interpretations are summarized in Table 1, where the deduced emplacement ages are reported.

- Samples from *group 1* contain no zircon cores and are characterized by a population of concordant U–Pb dates

that, with the exception of few outliers, are identical within uncertainties (Fig. 4). Therefore, the Concordia dates calculated from such data can be considered as representative of the emplacement age for samples of this group. This includes the KCG samples OL-13-24 (321.2 ± 1.4 Ma) and PRC-56 (332.1 ± 0.7 Ma) as well as vaugnerite samples 533-1 (307.8 ± 1.6 Ma), LR-31 (299.1 ± 1.3 Ma), LR-32 (301.5 ± 1.4 Ma), SC-13-02A (313.2 ± 2.5 Ma), SC-13-09 (309.7 ± 1.2 Ma), SC-13-19 (333.9 ± 1.4 Ma), SGC-12-13 (306.6 ± 2.4 Ma), SGC12-26 (306.1 ± 1.3 Ma), SGC-12-39 (306.6 ± 1.6 Ma) and SGC-12-42 (305.9 ± 1.7 Ma). Zircons from these samples can be considered as essentially undisturbed by any post-magmatic event.
- Zircon analyses in samples from *group 2* yield Carboniferous dates that are generally concordant within uncertainty, but cannot be combined into a single date, as they show a wide range in $^{206}Pb/^{238}U$ ratios (Fig. 5). Such zircons, or at least part of them, most probably underwent post-magmatic disturbance of the U–Pb isotopic system. This likely took place through diffusion, fluid-driven dissolution–recrystallization or diffusion–reaction processes (Gerdes and Zeh 2009) such that the resulting scatter in $^{206}Pb/^{238}U$ dates can be explained by variable extent of radiogenic Pb loss (Fig. 5). This assumption is supported by (i) the fact that most samples have lower intercept ages at about zero within uncertainty; and (ii) the observation that the analyses with the youngest $^{206}Pb/^{238}U$ dates often correspond to U-rich, metamict domains and/or porous zones rich in common Pb (Figs. 3, 5; see also Supplementary Material) that are particularly prone to Pb loss (Mezger and Krogstad 1997; Geisler et al. 2001). Following this interpretation, the upper intercepts of these "Discordia" trends should represent the crystallization age of the samples. This upper intercept date is always identical within uncertainties to the (more precise) Concordia date calculated by using the equivalent analyses with the highest $^{206}Pb/^{238}U$ ratios (Figs. 5, 6). The latter is thus considered as the best estimate for the crystallization age of the samples. This interpretation applies to the CPG sample OL-13-06 (312.9 ± 2.0 Ma), the KCG samples PMV (302.5 ± 0.9 Ma), SDZ (337.4 ± 1.0 Ma) and SGC-12-49B (298.9 ± 1.8 Ma) as well as the vaugnerite samples 533-2 (307.3 ± 1.3 Ma), PRC-53 (318.9 ± 1.8 Ma), PRC-54 (320.5 ± 1.8 Ma), SC-13-05 (309.4 ± 1.5 Ma) and SC-13-14 (335.7 ± 2.1 Ma).
- Finally, samples from *group 3* clearly contain complex zircon populations, in which the grains were formed by several, distinct crystallization events. This is well illustrated by core–rim relationships, with cores and rims having significantly different ages (Figs. 3a, 6). The most straightforward interpretation is that (i) zircon

cores represent either xenocrysts or crystals inherited from a zircon-bearing source material; and (ii) zircon rims, or grains devoid of any core, crystallized from the magma. The latter generally show the same distribution of U–Pb dates as zircon from samples of group 2, i.e., a range of apparent ^{206}Pb/^{238}U dates from a Carboniferous upper intercept and a lower intercept around zero. We thus apply the same interpretation as for group 2 samples, i.e., that such trends reflect the crystallization of zircon during emplacement of the host granitic magma, followed by recent loss of radiogenic Pb. This group includes all the MPG samples: HER (325.7 ± 1.3 Ma), OL-13-08 (311.0 ± 1.1 Ma) and OL-13-09 (312.7 ± 2.3 Ma); and most CPG samples: CHZ (332.0 ± 2.0 Ma), OL-13-11 (314.5 ± 1.7 Ma), OL-13-14 (318.3 ± 2.6 Ma), OL-13-21 (336.9 ± 1.8 Ma), TN-10 (321.9 ± 1.3 Ma), TN-19 (321.1 ± 1.1 Ma) and TOU-01 (322.2 ± 1.5 Ma).

- In three out of four investigated samples, monazite grains yielded Concordia dates that are identical within uncertainties to those deduced from zircon (sample OL-13-08: 309.3 ± 1.2 Ma; sample OL-13-11: 315.4 ± 0.9 Ma and sample OL-13-14: 317.8 ± 1.3 Ma; see Supplementary Material), which put further constraints on crystallization ages for these samples and supports our interpretation of the zircon U–Pb data. However, a notable exception is sample PRC-57, for which the monazite Concordia date is significantly younger (302.8 ± 1.3 Ma) than that of zircon (334.9 ± 1.5 Ma) (see Supplementary Material). This discrepancy might be explained by an inherited origin of all dated zircon grains, whereas monazite crystallized from the magma, as observed by Mougeot et al. (1997) and Couzinié et al. (2014) for other samples of the Velay granite. This interpretation is supported by (i) the fact that the ~335-Ma-old zircons of sample PRC-57 have identical ages, internal structures (bright CL luminescence, well-developed oscillatory zoning), and U–Th–Pb chemical compositions (150–500 ppm U,

Th/U = 0.5–1.0, no common Pb) as zircons of sample PRC-56, which forms an amphibole-bearing granodiorite (KCG) enclave within the same granite (few meters away of sample PRC-57), representing a plausible, nearby source for those zircons in the Velay granite; (ii) existing geochronological data on the Velay granite, clustering around 305–300 Ma (Caen-Vachette et al. 1982; Mougeot et al. 1997; Couzinié et al. 2014); and (iii) the fact that vaugnerite enclaves in the Velay granite at the same locality (PRC-53 and PRC-54) show significantly younger and robust U–Pb zircon ages (~320 Ma) than that obtained from PRC-57 (~335 Ma), showing that the latter cannot reflect the age of the Velay granite. The monazite Concordia age of 302.8 ± 1.3 Ma is thus interpreted as reflecting the crystallization of sample PRC-57.

Emplacement ages: comparison with published data

1. *CPG* The age of 332 Ma obtained for the Chalmazel granite (sample CHZ) is identical within uncertainties to that of the neighboring Bois-Noirs CPG pluton (341 ± 15 Ma, U–Pb ID-TIMS on zircon; Kosztolanyi 1971). In the same area, our age of 337 Ma for the Saint-Dier granite (sample OL-13-21) is consistent with the existing, but imprecise Rb–Sr whole-rock isochron age of 330 ± 26 Ma for this pluton (Saint-Joanis 1975).
   Further south, the ages of 315 and 318 Ma, respectively, obtained for the (undated so far) Almance and Chaise-Dieu laccoliths (samples OL-13-11 and OL-13-14) are within uncertainties of the ages obtained on intrusive pophyritic monzogranite and leucogranite in the nearby Livradois area (U–Pb LA-ICP-MS zircon ages of 315 ± 4 and 311 ± 18 Ma, respectively; Gardien et al. 2011).
   The age of the Margeride granite (OL-13-06; ~313 Ma) is identical within uncertainties to existing monazite ID-TIMS ages for the same granite (314 ± 3 Ma; Pin Pin 1979b), the associated Chambon-le-Château pluton (311 ± 6 Ma; Isnard 1996) and a whole-rock Rb–Sr isochron age of 323 ± 12 Ma (Couturié and Caen-Vachette 1979). It is, however, significantly younger than the U–Pb zircon age of 334 ± 9 Ma (ID-TIMS) obtained by Respaut (1984) on the Margeride granite.
   The ages of ~320 Ma obtained on laccoliths from the eastern flank of the Velay dome (Tournon granite and associated intrusions; samples TN-10, TN-19 and TOU-01) are slightly younger than the Rb–Sr whole-rock isochron age of 337 ± 13 Ma obtained by Batias and Duthou (1979), but their data also include samples from the Vienne pluton further north, for which no zircon age is available.
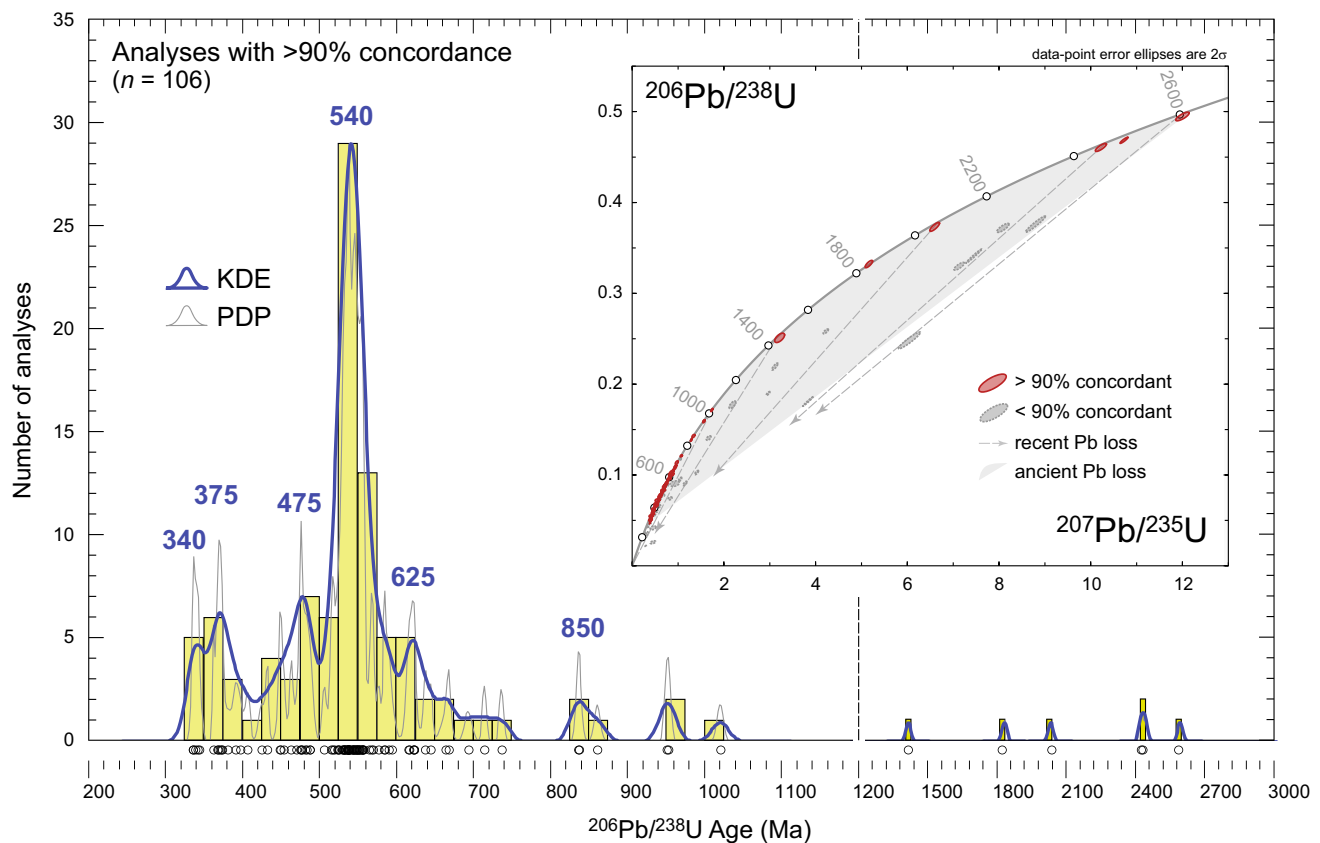
Fig. 7 Histogram (25 Ma bins), probability density plot (PDP) and Kernel Density Estimate (KDE) of $^{206}Pb/^{238}U$ ages for >90% concordant analyses of zircon cores from the eastern FMC granites (obtained using the density plotter program of Vermeesch 2012). The main peaks are identified using the KDE curve and labeled according to their average age. *Inset* Concordia diagram ($^{206}Pb/^{238}U$ vs. $^{207}Pb/^{235}U$) for all analyses from inherited zircon cores, including discordant ones

Finally, the monazite age of 302.8 ± 1.3 Ma obtained from the Velay granite at the Pont-Rouge quarry (sample PRC-57) is in line with the existing data obtained by different methods, including whole-rock Rb–Sr (Caen-Vachette et al. 1982) and monazite U–Th–Pb dating by ID-TIMS (Mougeot et al. 1997) or LA-ICP-MS (Couzinié et al. 2014), all pointing to crystallization ages in the range 305–300 Ma.

2. *MPG* In the northern part of the study area, the age of 327 Ma obtained for the Hermitage granite (sample HER) is identical to a whole-rock Rb–Sr isochron age of 329 ± 14 Ma (C. Pin, unpublished data mentioned in Didier et al. 1989). This age also complies with structural observations, since the Hermitage granite is a syn-kinematic intrusion emplaced along a WNW–ESE-trending dextral, strike-slip shear zone attributed to the D_3 deformation event (Barbarin 1983) that was most likely active at ~327 Ma, in agreement with a general NW–SW-directed stretching recorded throughout the FMC at that time (Faure et al. 2009).

In the Margeride area, the U–Pb ages of 311–309 and 313 Ma obtained for the Grandrieu leucogranite (sample OL-13-08) and Saint-Christophe-d'Allier pluton (sample OL-13-09), respectively, overlap with existing U–Pb ID-TIMS monazite ages of 305 ± 14 (Isnard 1996) and 305 ± 9 Ma (Lafon and Respaut 1988) for those two intrusions. Our ages are also identical within uncertainties to that of the Margeride granite (Table 1), which is crosscut by the Grandrieu granite in the field. This means that the two magmatic events were close enough in time such that they cannot be distinguished with respect to analytical uncertainties.

3. *KCG* The age of 337.4 ± 1.0 Ma obtained for the Salt-en-Donzy pluton (sample SDZ) is the first to document the absolute age of this intrusion. It is identical to whole-rock Rb–Sr isochron ages of 339 ± 8 and 322 ± 32 Ma obtained from granites flanking NE–SW-trending dextral shear zones in the Lyonnais mountains (Gay et al. 1981) and close to the ages of vaugnerite samples obtained from the same area (336–334 Ma;

see below). For the Saint-Julien-la-Vêtre pluton (sample SJV), the obtained age of 330.1 ± 1.3 Ma is consistent with an early Rb–Sr whole-rock isochron age of 340 ± 20 Ma (C. Pin, unpublished data quoted in Didier et al. 1989) and field relationships, since the pluton is intruded by the significantly younger (325.7 ± 1.3 Ma-old) Hermitage granite (Barbarin 1983; Didier et al. 1989).

The age of ~321 Ma obtained for the Gumières quartz–diorite (sample OL-13-24) is notably older than that obtained by Cocherie (2007) using the same technique (313 ± 2 Ma; U–Pb LA-ICP-MS on zircon). Excluding dating problems, this discrepancy might result from sampling of different lithologies in the composite Gumières Massif, which consists of porphyritic granodiorite associated with minor quartz–diorite, equigranular granite and dikes of the surrounding Velay granite (Barbarin et al. 2012). The sample dated by Cocherie (2007) may derive from the dominant biotite-bearing porphyritic granodiorite, whereas our sample is clearly more mafic (amphibole-bearing) and would thus derive from a dioritic enclave within this granodiorite, which are common yet not easy to identify given the scarcity of exposed contacts (Barbarin et al. 2012).

Another enclave within the Velay granite, sample PRC-56, yielded an age of 332.1 ± 0.7 Ma that is roughly equivalent to that of a suite of orthoclase-rich granites cropping out along the eastern margin of the Velay complex in the Vivarais area, dated at 353 ± 21 Ma (Rb–Sr whole-rock isochron) and 341 +8/–5 (U–Pb ID-TIMS on zircon, upper intercept age with two subconcordant spots at ~335 Ma) (Briand et al. 2002).

To the south of the Velay complex, in the Cévennes area, the age of 299 Ma obtained on sample SGC-12-49B from the Largentière granite is identical within uncertainties to that obtained by Couzinié et al. (2014) for the same granite (304.1 ± 6.3 Ma; U–Pb LA-ICP-MS on zircon) and also close to that of sample PMV from the Pont-de-Montvert pluton (302.5 ± 0.9 Ma). Both ages are identical within uncertainties to ages of 301 ± 4 and 307 ± 11 Ma (zircon and monazite U–Pb ID-TIMS) in the Mont-Lozère and Aigoual granitic complexes (Brichau et al. 2008; François 2009). Moreover, they overlap with Ar–Ar ages of 306–301 Ma obtained from aplitic–pegmatitic dykes and Au-mineralized quartz veins in the vicinity of the Mont-Lozère complex (Chauvet et al. 2011).

4. *Vaugnerites* Our new age data suggest that the vaugnerites in the eastern FMC intruded over >35 Ma, between 335.7 ± 2.1 Ma (SC-13-14) and 299.1 ± 1.3 Ma (LR-31). This period is much longer than previously suggested (Aït-Malek 1997; Couzinié et al. 2014). In the northern part of the study area, the new emplace-

ment ages of ~335 Ma for the syn-kinematic vaugnerite dikes/bodies in the Lyonnais area (SC-13-14 and SC-13-19) are consistent with existing Rb–Sr data of 339 ± 8 and 322 ± 32 Ma obtained from nearby (and, as shown by magma mixing relationships, coeval) granites (Gay et al. 1981).

In the western and central parts of the Velay complex, no absolute ages were available so far for vaugnerite intrusions. Our results from samples in this area show emplacement ages scattered over more than 20 Ma, and specifically clustered at 321–319 Ma (age of the two quartz–syenite enclaves within the Velay granite at Pont-Rouge (PRC-53 and PRC-54), 310 Ma (Pubellier syenodiorite, SC-13-09) and 302–299 Ma (diorite enclaves in the Velay granite; LR-31 and LR-32).

Two vaugnerite enclaves within the Margeride batholith (SC-13-02a and SC-13-05) yielded ages (313–309 Ma) that are identical within uncertainties to the emplacement age of the surrounding Margeride granite (312.9 ± 2.0 Ma; sample OL-13-06), supporting field observations indicating that the vaugnerites are coeval with the granite.

Finally, to the south of the Velay complex, vaugnerite samples from Loubaresse (SGC-12-39) and Meyras (SGC-12-42) yield ages of 306.6 ± 1.6 and 305.9 ± 1.7 Ma, respectively, which are identical to those of Couzinié et al. (2014) for the same vaugnerite bodies (307.4 ± 1.8 and −305.8 ± 2.3 Ma, respectively; U–Pb zircon by LA-ICP-MS). The age obtained on the Meyras vaugnerite is also identical to that of Aït Malek (1997) (308 ± 6 Ma; U–Pb zircon by ID-TIMS), but this author obtained a significantly older age for the Loubaresse vaugnerite (313 ± 3 Ma; see Couzinié et al. 2014 for discussion). The Pont-de-Bayzan vaugnerite gave an emplacement age of 306.1 ± 1.3 Ma (SGC-12-26). This age is significantly older than the age of 294.4 ± 3.9 Ma published by Couzinié et al. (2014) from the same outcrop, but from a different vaugnerite body. The latter, Permian age would not reflect the crystallization age, due to perturbation of the zircon U–Pb isotopic system by fluid–rock interactions (Couzinié et al. 2014).

Significance of inherited zircon ages

Zircon xenocrysts from CPG and MPG reveal an age spectrum characterized by abundant early Paleozoic to Neoproterozoic ages between ~450 and ~740 Ma (with more prominent peaks at ~475, ~540 and ~625 Ma), together with very minor Grenville (955–1025 Ma) and Paleoproterozoic to early Archean ages (1800–2600 Ma) (Fig. 7). Such an age spectrum is similar to that of zircons from ortho- and paragneisses of the UGU and LGU in the FMC

(Melleton et al. 2010; Chelle-Michou et al. 2015), which are the country rocks and, most likely, the sources of CPG and MPG (Williamson et al. 1996, 1997; Downes et al. 1997; Barbey et al. 1999, 2015). Thus, it is clear that these zircons were inherited from the regional nappe units, either during melting or emplacement.

The observed age spectrum is very similar to the age distribution of detrital zircons from many Paleozoic (Cambrian to Devonian) sedimentary rocks throughout western Europe (Zeh et al. 2001; Kober et al. 2004; Linnemann et al. 2004, 2007, 2014; Gerdes and Zeh 2006) and has also been reported in inherited zircons from Variscan granites of the Iberian Massif (Castiñeiras et al. 2008; Fernández-Suárez et al. 2011). This age distribution is generally interpreted to reflect zircon derived from the Avalonian-Cadomian belt (and its cratonic hinterland), forming a ca. 10,000-km-long cordillera at the northern margin of Gondwana during Neoproterozoic to Cambrian times (see Nance et al. 1991; Nance and Murphy 1994; Fernández-Suárez et al. 2000; Zeh et al. 2001; Linnemann et al. 2014; and references therein). During the early Ordovician (490–470 Ma), this cordillera became dispersed, with individual microterranes (e.g., Avalonia, Amorica, Alpine terranes, etc.) drifting to the north and re-assembled subsequently during the Variscan orogeny at 360–320 Ma (Nance et al. 2002; von Raumer et al. 2002; Linnemann et al. 2007; Faure et al. 2009; Stampfli et al. 2013). The age peaks of the inherited zircons from the eastern FMC granitoids can be ascribed to several well-known events throughout this evolution, notably the formation of an arc-back-arc system at ca. 660–560 Ma; its evolution into an Andean-type continental margin at 550–530 Ma and its subsequent breakup at 530–480 Ma, resulting in the opening of the Rheic Ocean (see Ballèvre et al. 2001; Nance et al. 2002, 2010; Linnemann et al. 2004, 2007 and references therein). The two youngest peaks at middle Devonian (390–370 Ma) and early Carboniferous ages (360–340 Ma) correspond respectively to subduction processes related to the closure of the Rheic Ocean (Zeh and Gerdes 2010) and to the Variscan collision (Faure et al. 2009). The latter period is characterized by important crustal melting, granulite-facies metamorphism (Duthou et al. 1994; Gardien et al. 2011) and emplacement of arc-like, calc-alkaline gabbros and granitoids in the Morvan and Limousin areas (Bernard-Griffiths et al. 1985; Pin and Paquette 2002).

Zircon constraints on granitoid petrogenesis

Zircon constraints on CPG and MPG petrogenesis

These granitoids contain abundant, rounded to subhedral zircon cores with pre-Variscan ages, commonly wrapped by rims formed during the Variscan magmatic episode

(Figs. 3, 6 and 7). These characteristics are in good agreement with previous interpretation that the MPG and CPG are of crustal origin (Williamson et al. 1996, 1997; Downes et al. 1997; Barbey et al. 1999) and formed at relatively low temperatures, specifically below magmatic Zr saturation. Considering that the pre-Variscan zircons in CPG and MPG were inherited from the source rock during melting, Zr saturation temperatures would provide a first-order estimate of *maximum* magma temperatures. These temperatures, calculated using the Zr saturation thermometer of Watson and Harrison (1983), are in the range 720–787 °C for the MPG and 761–842 °C for CPG (Fig. 8). Such values are consistent with results of previous melting experiments carried on metasedimentary rocks at mid-crustal pressures (Vielzeuf and Holloway 1988; Patiño-Douce and Johnston 1991; Gardien et al. 1995; Patiño-Douce and Harris 1998; Pickering and Johnston 1998), which produced granitic liquids that match the compositions of CPG and MPG at 700–850 °C (Fig. 8). The generally lower Zr saturation
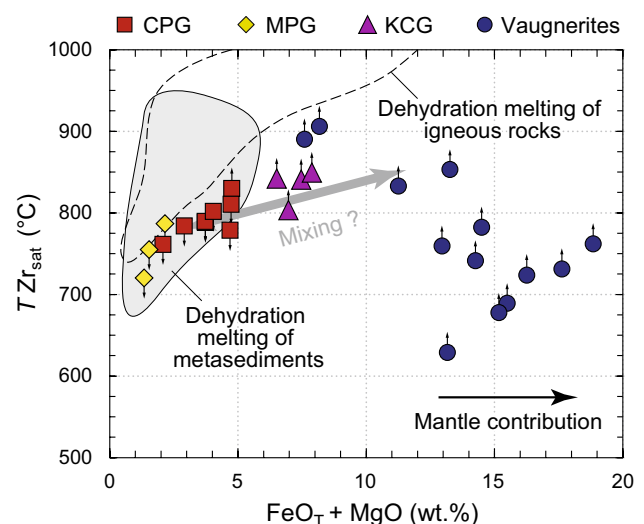

Fig. 8 Plot of the zircon saturation temperature ($T\,Zr_{sat}$, in °C) obtained from the whole-rock compositions of the dated samples of Variscan igneous rocks from the eastern FMC (using the equation of Watson and Harrison 1983), as a function of their "mafic" oxides contents ($FeO_t + MgO$). The fields correspond to the temperature and compositions of experimental melts of Gardien et al. (1995), Patiño-Douce and Harris (1998), Patiño-Douce and Beard (1995, 1996), Patiño-Douce and Johnston (1991), Pickering and Johnston (1998), Vielzeuf and Holloway (1988) and Vielzeuf and Montel (1994) for metasediments; Beard and Lofgren (1991), Bogaerts et al. (2006), Patiño-Douce and Beard (1995), Rapp and Watson (1995), Rapp et al. (1991), Singh and Johannes (1996), Sisson et al. (2005), Skjerlie and Johnston (1996); Tatsumi and Suzuki (2009), Watkins et al. (2007) and Wolf and Wyllie (1994) for igneous rocks. The arrows associated with the symbols indicate whether the calculated $T\,Zr_{sat}$ represents maximum magma temperatures (*arrow down*, if source-inherited zircons are present) or minimum ones (*arrow up*, few or no inherited zircons)

Fig. 9 Histograms and Kernel Density Estimates (KDE) (obtained ▶ using the DensityPlotter program of Vermeesch 2012) of $^{206}Pb/^{238}U$ ages of zircons from **a** orthogneisses and **b** paragneisses of the FMC (data from Melleton et al. 2010; Chelle-Michou et al. 2015; Mintrone 2015); compared to inherited zircons from (**c**) CPG and (**d**) MPG investigated in this study. Only analyses with >90% concordance and with $^{206}Pb/^{238}U$ ages <1200 Ma are considered. The gray fields in **c** and **d** are the KDE of age distributions for zircons of ortho- and paragneisses presented in (**a**) and (**b**); the *dashed blue curve* represent the KDE obtained with all zircons from both ortho- and paragneisses together

temperatures obtained for the MPG could be explained either by water-present melting (Williamson et al. 1996) or muscovite breakdown melting (720–770 °C at 7 kbar; Patiño-Douce and Harris 1998). In contrast, the higher temperatures obtained for the CPG exceed that of muscovite dehydration melting and thus require biotite dehydration melting (800–870 °C; Vielzeuf and Montel 1994; Patiño-Douce and Beard 1995, 1996), in good agreement with the previous interpretations of Barbey et al. (1999, 2015) and Moyen et al. (in press).

On the other hand, the respective contribution of pre-Variscan ortho- and paragneisses of the FMC in the source of MPG and CPG is the matter of several discussions (Turpin et al. 1990; Williamson et al. 1996, 1997; Downes et al. 1997; Moyen et al. in press). It is worthwhile noting that ortho- and paragneisses of the FMC reveal important differences in their age spectra. Zircon grains from the orthogneisses show two prominent age peaks at ~475 Ma (early Ordovician) and ~540 Ma (early Cambrian) (Fig. 9a), corresponding to the magmatic ages of their respective protoliths (Caen-Vachette 1979; Pin and Lancelot 1982; Duthou et al. 1984; Lafon 1986; R'Kha Chaham et al. 1990; Alexandrov et al. 2001; Alexandre 2007; Melleton et al. 2010; Chelle-Michou et al. 2015; Mintrone 2015), whereas detrital zircons from the paragneisses show the same peak at 475 Ma, in addition to a wide Neoproterozoic age cluster between 560 and 650 Ma, with a distinctive "tail" until 1000 Ma (Fig. 9b) (Melleton et al. 2010; Chelle-Michou et al. 2015). The inherited zircon age spectra of both CPG and MPG (Fig. 9c, d) are intermediate between those two end-members, with a prominent age peak at ~540 Ma like in orthogneisses together with a significant number of Neoproterozoic zircon grains (mostly at 560–650 and up to 1000 Ma), typical of paragneisses (Fig. 9c, d).

A striking difference, though, is the limited number of Ordovician (~475 Ma) inherited zircons in the CPG and MPG, as already noted in the case of the Velay granite (Couzinié et al. 2014; Chelle-Michou et al. 2015). It must be
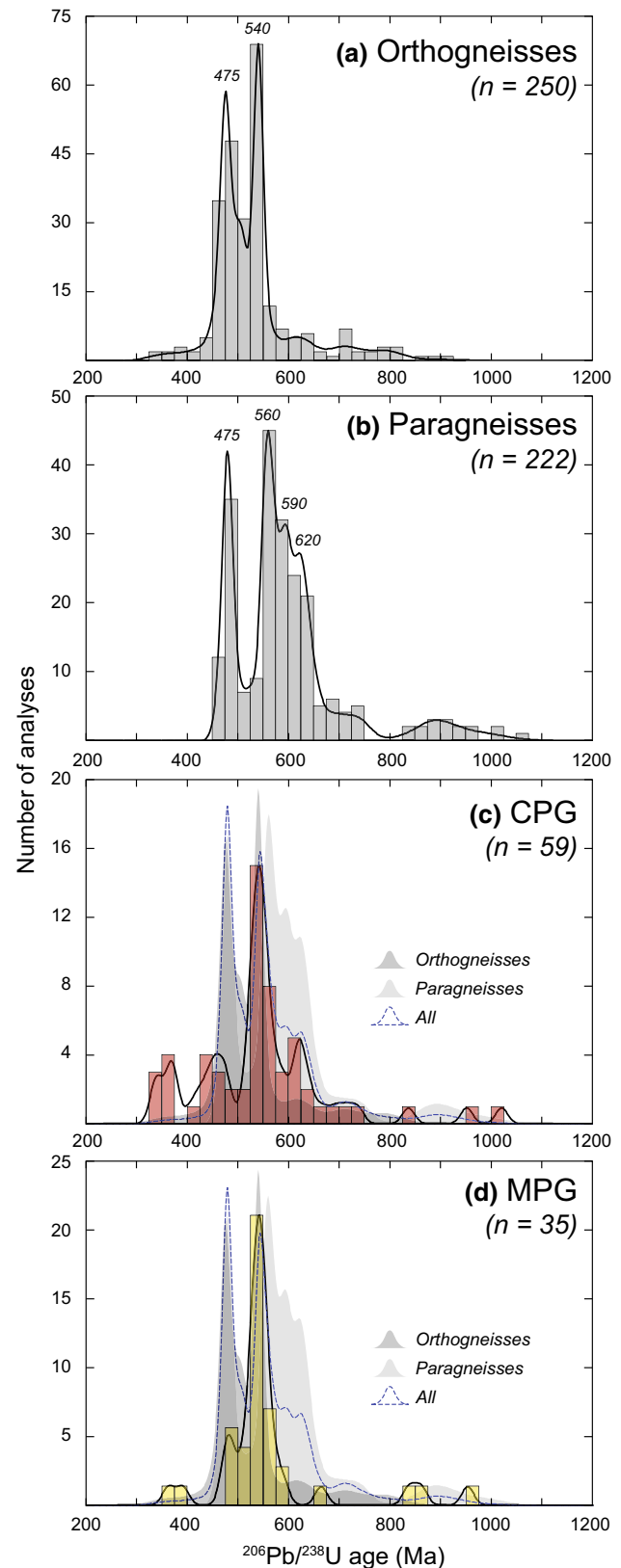
emphasized that the age spectra presented in Fig. 9 for the MCF ortho- and paragneisses result from the compilation of data from all lithostratigraphic units (PAU, UGU, LGU) and both the eastern and western parts of the FMC. In fact, there are clear differences in the zircon age distributions between the UGU and LGU in the eastern FMC, the most relevant one being that Ordovician ages are restricted to the UGU and LAC (Pin 1979a; Pin and Lancelot 1982; Chelle-Michou et al. 2015) whereas in the LGU, both the youngest detrital zircon grains in paragneisses and the magmatic protoliths of orthogneisses have Cambrian ages at 545–520 Ma (Caen-Vachette 1979; Duthou et al. 1984; R'Kha Chaham et al. 1990; Chelle-Michou et al. 2015; Mintrone 2015). We therefore interpret the limited number of Ordovician inherited zircons from the CPG and MPG to reflect a source region rooted in the LGU, where zircons younger than 520 Ma are scarce.

All lines of evidence suggest that the source of both CPG and MPG consists of a mixed assemblage of para- and orthogneisses from the LGU. The CPG (including the Velay granite) formed by biotite dehydration melting at high temperature (≥800 °C), whereas MPG formed at lower temperature (<800 °C) through muscovite breakdown or water-present melting.

Zircon constraints on KCG and vaugnerite petrogenesis

Xenocrysts in KCGs and vaugnerites are very scarce ($n = 9$, among 21 samples). The estimated Zr saturation temperatures for these rocks are ≤850 °C (Fig. 8), i.e., much lower than presumed magma temperature for vaugnerites (>1000 °C; Montel and Weisbrod 1986), which may indicate that potential zircon xenocrysts in the magma were dissolved because of Zr undersaturation. These potential xenocrysts were probably assimilated from the wallrock in which the mafic magma percolated (e.g., in sample SC-13-14), rather than inherited from a crustal source. These magmas indeed have "crust-like" trace element and Nd–Hf isotopic compositions, yet their very high $FeO_t + MgO$ (most often >10 wt%; Fig. 8) and low SiO_2 contents preclude either a crustal origin or crustal contamination of a basaltic melt (Turpin et al. 1988; Couzinié et al. 2016). Instead, vaugnerites are more likely to be derived from an "enriched" mantle source metasomatized by 10–25% of crust-derived materials (see Couzinié et al. 2016 for a more detailed discussion about the origin of these rocks).

A crust-dominated origin for the KCGs is precluded by their high $FeO_t + MgO$ contents (>6 wt%) that would require an igneous mafic source (amphibolites, which are scare in the LGU) and melting temperatures ≥950 °C (Fig. 8) that are unrealistically high (Moyen et al. in press). These observations could indicate that KCG derive from interactions (mixing, mingling) between Zr-saturated crustal melts (similar to CPG and MPG) and a hot, mantle-derived, Zr-undersaturated vaugnerite magma (Downes et al. 1997; Solgadi et al. 2007), thereby triggering the partial to total dissolution of inherited zircons. Such mixing between vaugnerites and CPG/MPG is supported by the intermediate composition of KCG between the two end-members (Figs. 2, 8). Alternatively, the high SiO_2 content of the KCG (~69 wt%) could be explained also by a high degree of fractionation of vaugnerite magma, in agreement with the close spatial and petrographic relationships between these rocks (Barbarin 1988) and geochemical constraints (Moyen et al. in press). In either case, the involvement of mantle-derived, vaugnerite magma is required to explain the composition of the KCG.

The Carboniferous thermal anomaly in the eastern FMC: evidence for lithospheric mantle delamination

Our new geochronological data indicate that the late-Variscan plutonic rocks of the eastern FMC emplaced between ~339 and ~298 Ma (when uncertainties are considered) (Fig. 10). This dataset thus represents the first, self-consistent and unambiguous evidence that magmatic activity lasted throughout the entire late Carboniferous for ~40 Ma, as proposed by earlier studies (Vanderhaeghe et al. 1999; Vanderhaeghe and Teyssier 2001; Ledru et al. 2001; Rossi and Pin 2008; Faure et al. 2009). The estimated timescales for the magmatism in the FMC are much longer than those assessed for the evolution of magma from source to emplacement (production, segregation, ascent and crystallization) that commonly lasts no more than 5 Ma (Harris et al. 2000; Petford et al. 2000; Annen et al. 2006; Walker et al. 2007; de Saint-Blanquat et al. 2011). Thus, the ~40-Ma-long magmatism necessarily implies the existence of a long-lived thermal anomaly, to sustain a high heat flux and crustal anatexis throughout the Carboniferous (Rossi and Pin 2008; Vanderhaeghe 2012).

In fact, such a protracted Carboniferous thermal anomaly in the eastern FMC was already suggested on the basis of studies on metamorphic rocks, indicating an early, M_3-metamorphic episode characterized by incipient partial melting of the metamorphic nappe pile at P–T conditions of 5–6 kbar and 720–750 °C between ~330 and ~310 Ma (Montel et al. 1992; Mougeot et al. 1997; Barbey et al. 1999, 2015; Cocherie et al. 2005; Bé Mézème et al. 2006; Bouilhol et al. 2006), followed by biotite dehydration melting at P–T conditions of 4–5 kbar and 750–850 °C at 305–301 Ma (M_4-metamoprhic episode; Caen-Vachette et al. 1982; Montel et al. 1992; Mougeot et al. 1997; Barbey et al. 1999, 2015; Couzinié et al. 2014). The M_4 event required a higher apparent geothermal gradient than the M_3 episode and corresponds to the formation of the Velay granite–migmatite dome. In the past, limited partial melting during the M_3 episode
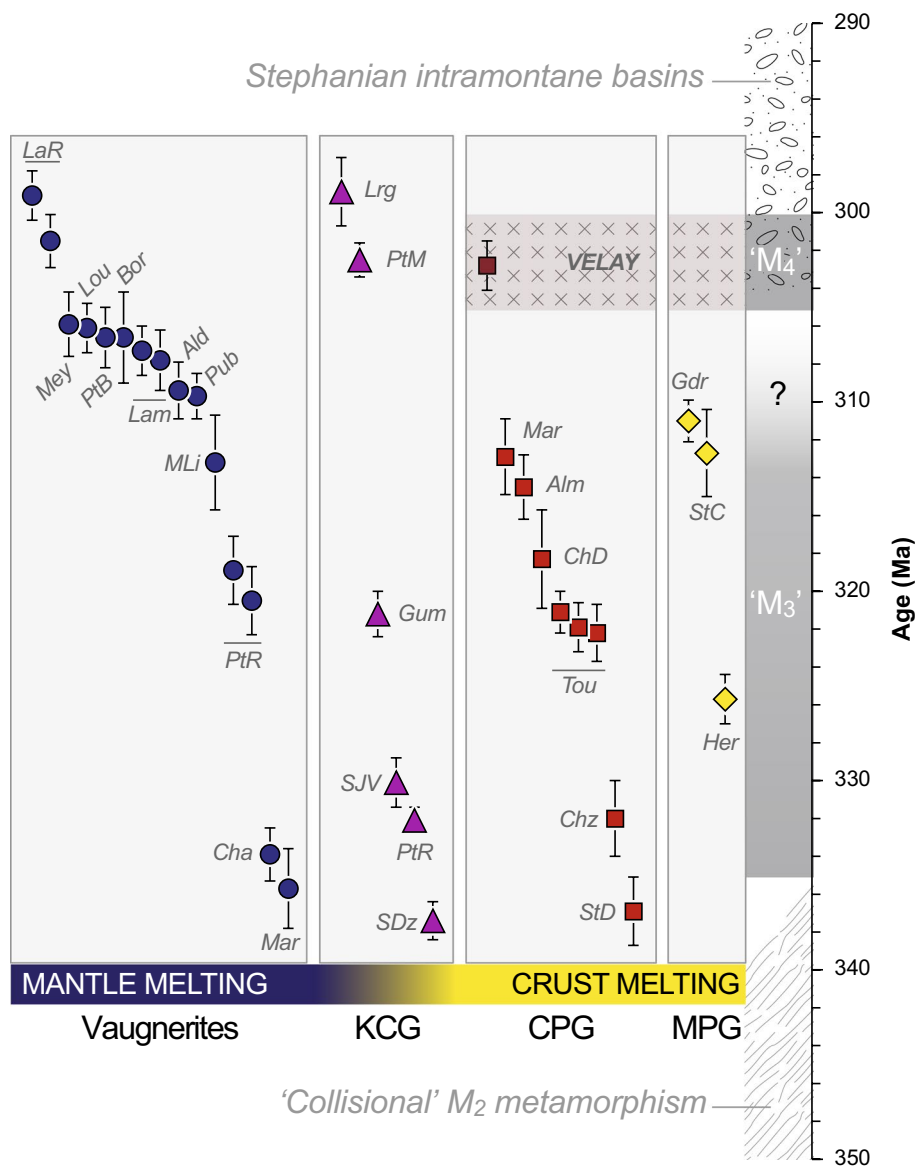
Fig. 10 Timeline summarizing all the intrusion ages obtained for Variscan igneous plutonic rocks from the eastern FMC in the course of this study (symbols are as in Figs. 2, 8). The groups of samples (CPG, MPG, KCG and vaugnerites) are sorted according to the respective contribution of crustal and mantle sources to their petrogenesis (see "Discussion"). On the right-hand side are represented major time markers in the Variscan evolution of the eastern FMC, including collision-related M₂ metamorphism (Gardien 1990; Caron 1994; Faure et al. 2009; Melleton et al. 2009; Schulz 2014), the two anatectic episodes M₃ and M₄—the latter being related to the development of the Velay dome (Montel et al. 1992; Barbey et al. 1999, 2015; Couzinié et al. 2014) and development of "Stephanian" (upper Pennsylvanian), intramontane coal-bearing basins (Malavieille et al. 1990; Faure et al. 2009). Abbreviations are for the names of the dated intrusions: *Ald* L'Aldeyrès, *Alm* Almance, *Bor* Borne, *Cha* Chassagny, *ChD* Chaise-Dieu, *Chz* Chalmazel, *Gdr* Grandrieu, *Gum* Gumières, *Her* Hermitage, *Lam* Lamastre, *LaR* La Roche, *Lou* Loubaresse, *Lrg* Largentière, *Mar* Margeride, *Mey* Meyras, *MLi* Moulin de Linas, *Mrc* Marcenod, *PtB* Pont-de-Bayzan, *PtM* Pont-de-Montvert, *PtR* Pont-Rouge quarry, *Pub* Pubellier, *SDz* Salt-en-Donzy, *SJV* Saint-Julien-la-Vêtre, *StC* Saint-Christophe-d'Allier, *StD* Saint-Dier-d'Auvergne, *Tou* Tournon and associated intrusions

has been attributed mainly to enhanced radioactive heat production, due to accumulation of radioactive elements in the over-thickened orogenic crust (e.g., Vanderhaeghe et al. 1999; Rossi and Pin 2008), possibly coupled to limited heat advection from the intrusion of vaugnerites. The higher, apparent geothermal gradient during the

M₄ episode was assumed to result from two factors: first, the transfer of magmas from lower/middle to upper crustal levels during the formation of the Velay dome (Barbey et al. 2015), and second, the emplacement of mantle-derived (vaugnerite) melts (Williamson et al. 1992, 1997; Ledru et al. 2001; Rossi and Pin 2008).

Three problems, however, rise from these hypotheses:

1. As pointed out by Barbey et al. (2015), M_3 melting was necessarily more intense in the lower crust than it is recorded at the present level of exposure, in order to explain the formation and emplacement of the widespread 337–312-Ma-old CPG plutons (Fig. 10) for the origin of which biotite dehydration melting ($T > 800\ °C$) is required.

2. The geochronological data obtained in this study show that vaugnerites ± KCG (338–298 Ma) and CPG + MPG (339–302 Ma) emplaced synchronously throughout the Carboniferous (Fig. 10), rather than successively, as would be expected if crustal melt production was caused by mafic magmatic underplating (first vaugnerites ± KCG, second CPG + MPG ± KCG).

3. Thermal modeling indicates that crustal melt productivity induced by heat advection from the intrusion or underplating of mantle-derived basalt rarely exceeds 10% of the whole volume of mafic magma (Petford and Gallagher 2001; Annen and Sparks 2002; Annen et al. 2006). This entails that the volume of basalt must have been nine times larger than the final volume of crust-derived granites. In the case of the eastern FMC, such a high ratio appears unrealistic because vaugnerites are largely subordinate in volume relative to the granites (Couzinié et al. 2016). There is evidence from lower crustal xenoliths brought up by Cenozoic volcanoes that mafic igneous rocks are present in the lower crust of the eastern FMC (Dostal et al. 1980; Downes et al. 1990). However, available age constraints on these rocks suggest that they would represent a Permian (300–250 Ma-old) underplating event (Supply 1981; Costa and Rey 1995; Féménias et al. 2003) and could therefore not be responsible for the heat anomaly at the origin of Carboniferous magmatism.

Thus, mantle-derived magmas unlikely represent the main heat source for crustal melting and the genesis of the voluminous CPG and MPG, during neither M_3, nor M_4, and an alternative hypothesis must be sought. The close association in both space and time of crust-derived granites and vaugnerites in the eastern FMC suggests that they are all the "byproducts" of one-and-the-same, lithospheric-scale geodynamic process. This process would be ideally represented by lithospheric mantle delamination, accompanied by the ascent of hot (>1200 °C) asthenospheric mantle up to the crust–mantle boundary (Moho). Thermo-mechanical modeling (van Hunen and Allen 2011; Duretz and Gerya 2013; Magni et al. 2013) and geological observations from other orogenic systems (Black and Liégeois 1993; Coulon et al. 2002; Guo et al. 2013; Laurent et al. 2014b) show that this process is common at the final stages of continental

collision. Lithospheric mantle delamination was also suggested to explain the Carboniferous record in other parts of the Variscan belt (Henk et al. 2000; von Raumer et al. 2013; Denèle et al. 2014) and is backed by geophysical data, since the mantle underneath the eastern FMC is characterized by low P-wave velocities interpreted as reflecting the removal of the Variscan orogenic roots (Averbuch and Piromallo 2012). Thermal modeling demonstrated that an anomalously high heat flux through the Moho (equivalent to that of the convective mantle) triggers widespread lower crustal melting and magma transfer to the middle crust, accounting for high geothermal gradients and granulite-facies metamorphism (apparent geotherm of >50 °C km^{-1}) within 25–35 Ma (Depine et al. 2008). The increase in temperature is maximum in the case of conjunct crustal thickening enhancing radioactive heating and thinning of the lithospheric mantle causing an increase of the heat flux at the base of the crust (Vanderhaeghe and Duchêne 2010). This scenario is very consistent with geological and geochronological data from the eastern FMC showing the same incubation time between the intrusion of the first vaugnerites and granites at about 337 Ma and the rise of the Velay granite–migmatite dome at 310–300 Ma (Fig. 10) associated with the apparently higher-temperature "M_4" episode.

Consequences for the Variscan tectonic evolution of the eastern FMC

The magmatic rocks in the eastern FMC reveal a clear temporal vs. spatial evolution (Fig. 11). All magma types (CPG, MPG, KCG and vaugnerites) can indeed be found throughout the entire FMC, but their emplacement ages decrease systematically from north to south between 340 and 305 Ma (Fig. 11). The CPGs, KCGs and vaugnerites in the northernmost part of the FMC (Forez, Livradois and Lyonnais mountains) emplaced at 337 to 330 Ma; the youngest intrusion is represented by the Hermitage MPG pluton at ~326 Ma (Fig. 11). Further south, the CPG laccoliths that flank both the eastern (Tournon, Dunières) and western (Chaise-Dieu, Almance) sides of the Velay dome, as well as the large enclaves of CPG, KCG and vaugnerites in the latter, emplaced between 332 and 315 Ma, mostly at 320 Ma (Fig. 11). The Margeride batholith at the SW end of the Velay dome (the Margeride granite itself plus associated MPG and vaugnerites) intruded at 313–309 Ma; and finally, emplacement of the KCG plutons and abundant vaugnerites in the southernmost Cévénnes domain took place at even younger ages of 307–298 Ma (Fig. 11).

We propose that the observed zonal pattern results from the progressive, southward migration of the thermal anomaly, which was responsible for coeval and protracted crust- and mantle-derived magmatism. This migrating thermal anomaly can be explained by asymmetric delamination of
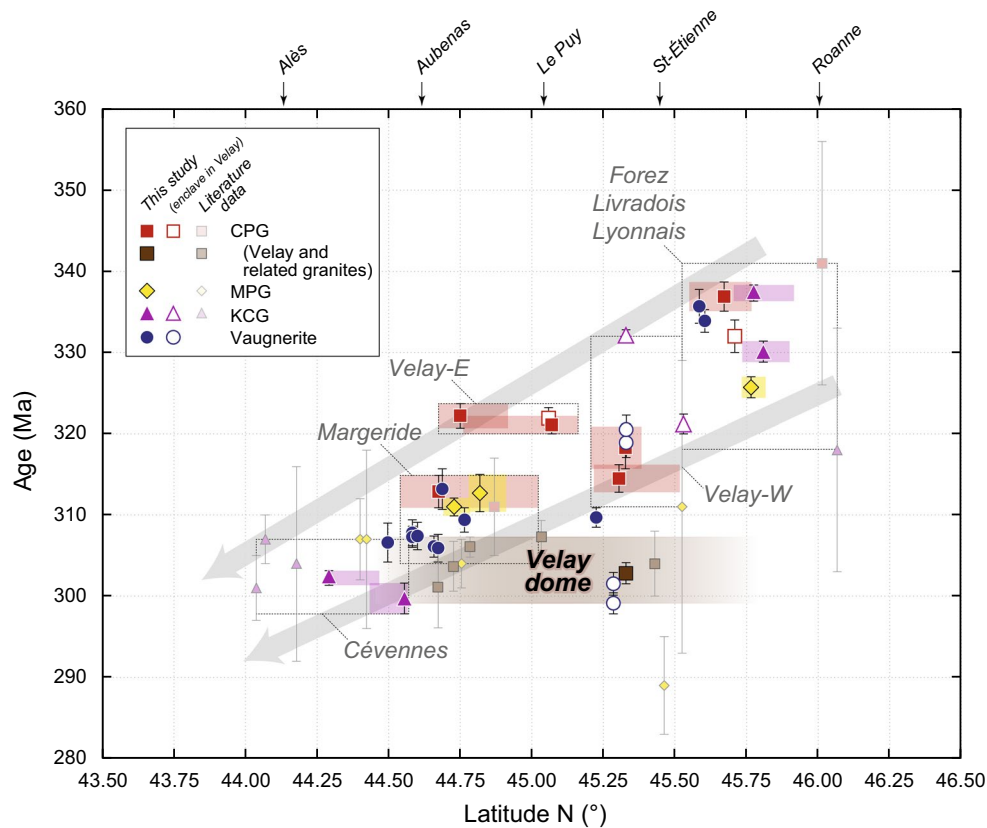
Fig. 11 Plot of the intrusion ages obtained for Variscan igneous rocks from the eastern FMC, as a function of the latitude (in decimal degrees) at which the samples were collected. The *colored boxes* represent individual plutons or batholiths (including the Velay dome); their horizontal extension is constrained by the geographic limits of the pluton, and their vertical extension by the age uncertainties obtained on dated samples from this pluton. The *dashed boxes* represent a group of plutons or intrusions that belong to the same geographic domain. The *light gray arrow* qualitatively highlights that the age of the oldest pluton/magmatic body in a given geographic area decreases southward (see "Discussion"), excluding the Velay dome which shows a relatively homogeneous age record across its entire surface. References are as in Table 1 with additional data from Barbarin et al. (2012) and Chelle-Michou et al. (2015) for the Velay granite and associated bodies

the subcontinental lithospheric mantle beneath the FMC, starting to the north and propagating southwards. Heat conduction from the inflowing asthenosphere triggered the partial melting of the lithospheric mantle enriched in incompatible elements during previous subduction (Couzinié et al. 2016; von Raumer et al. 2013) and caused formation of modest volumes of vaugnerite magmas. Such lithospheric mantle source could have either been part of the delaminating slab or represented by slivers that remained mechanically coupled to the lower crust during delamination. Concurrently, enhanced mantle heat flux through the Moho caused widespread lower crustal melting and the formation of granitic magmas (CPG + MPG). Interactions between those two magmatic end-members, and/or differentiation of vaugnerite magmas, led to the formation of KCG.

On the other hand, the granites and migmatites forming the core of the Velay complex span nearly the entire area covered by the other intrusions, but in contrast to the

latter reveal no age zoning. These rocks rather crystallized within a short period of time at 305–300 Ma, regardless the latitude (Fig. 11). Our new age of 302.8 ± 1.3 Ma from the Pont-Rouge quarry, in the central-northern part of the dome, is indeed within uncertainties of, or very close to, the monazite U–Pb ages of 301 ± 5 (Mougeot et al. 1997), 303.7 ± 3.1 and 305.9 ± 1.4 Ma (Couzinié et al. 2014) from its southern part; and the zircon U–Pb ages of 307.5 ± 2.0 Ma (Chelle-Michou et al. 2015) and 304 ± 4 Ma (Cocherie 2007) obtained in the eastern and northern edges of the complex, respectively. The lack of "age zoning" in the Velay dome at the temporal resolution of existing data suggests that it represents a partially molten, middle to lower crustal layer rapidly exhumed during the late Carboniferous (Vanderhaeghe et al. 1999). Prolonged lower to middle crust melting started above the widening "asthenospheric window," which was formed during progressive southward lithospheric mantle delamination. This caused a rheologic weakening of the lower crust,

which eventually led to lateral crustal flow, thinning and collapse of the orogenic crust, and the exhumation of the partially molten crust in the core of domes like the Velay complex (Vanderhaeghe and Teyssier 2001; Vanderhaeghe 2012). In this perspective, the 305–300 Ma age cluster obtained in the Velay granite and migmatites does not necessarily correspond to a "catastrophic" melting event (Couzinié et al. 2014). Instead, it simply reflects the final exhumation and cooling of these rocks below their solidus, as a natural outcome of the whole delamination process.

The occurrence of southward lithospheric mantle delamination in the eastern FMC during the Carboniferous can be considered in the scope of existing geodynamic scenarios for this part of the Variscan belt. Faure et al. (2009) stressed out that there are two possible, competing models that may explain the present-day structure of the FMC:

1. A "monocyclic" model (e.g., Lardeaux et al. 2001) considering a single, northward-directed subduction from the Silurian to the late Devonian. In this context, the suggested southwards lithospheric delamination wit-

nessed by the Carboniferous magmatic evolution could simply reflect the rollback of the lithospheric mantle (Fig. 12a), in response to decoupling with the overlying continental crust while convergence was still active (Vanderhaeghe and Duchêne 2010; Duretz and Gerya 2013; Magni et al. 2013).

2. A "polycyclic" model (e.g., Faure et al. 2005) in which northward-directed subduction during the Ordovician and early Silurian ("Eo-Variscan" cycle, Armorica–Gondwana collision) was followed by Devonian, southward-directed subduction that accommodated the closure of the Rheic Ocean ("Variscan" cycle, Laurussia-[Armorica + Gondwana] collision). In this case, thermo-mechanical models of mature continental collision suggest that if the lithospheric mantle of the lower (i.e., subducting) plate is retreating, it causes a "retro-delamination" of the lithosphere underneath the overriding plate and asthenospheric upwelling (Gray and Pysklywec 2012), equally accounting for southward lithosphere delamination under the eastern FMC (Fig. 12b).
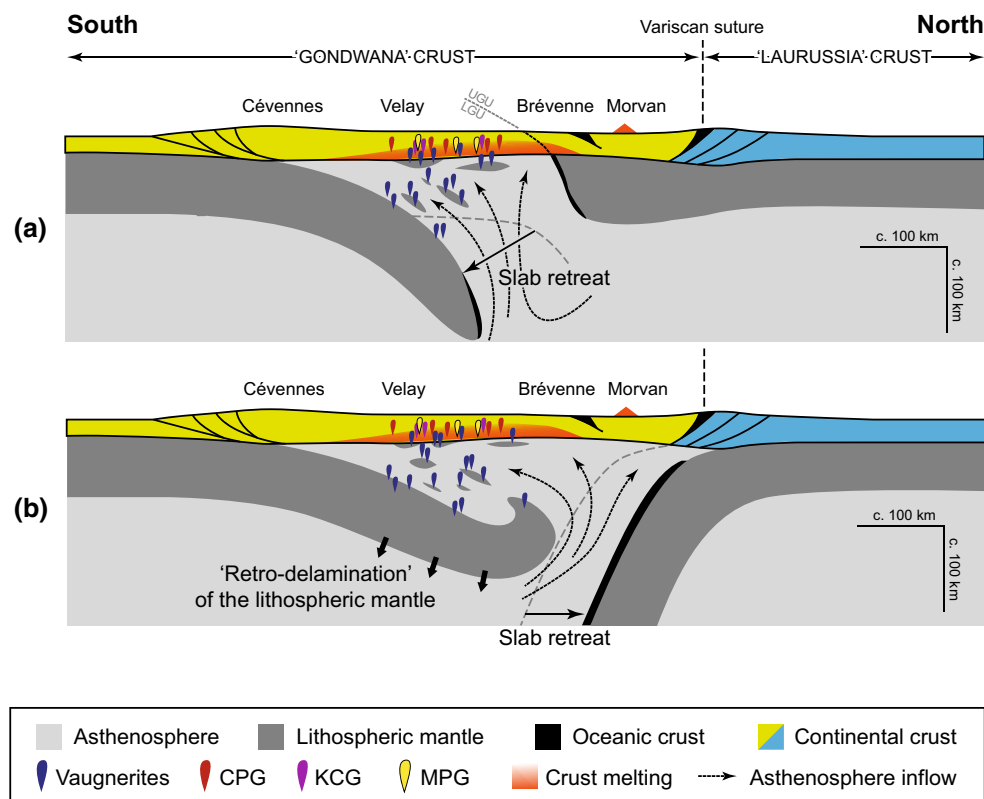
Fig. 12 Two possible, schematic geodynamic models that may account for the spatial and temporal distribution of Variscan igneous plutonic rocks in the eastern FMC during the Carboniferous (c. 340–300 Ma): **a** southward retreat of a lithospheric mantle slab, after middle Devonian (>360 Ma-old) subduction of continental crust now exhumed at the UGU/LGU boundary (highlighted by the *dashed line*); or **b** "retro-delamination" of the lithospheric mantle in response to slab retreat of the lower plate (i.e., the "Laurussia" plate) following collision (redrawn after Fig. 2c of Gray and Pysklywec 2012)

The two models have their strengths and weaknesses. The "monocyclic" model (Fig. 12a) is supported by the presence of (U)HP rocks at the base of the UGU (late Devonian migmatites with embedded eclogite boudins) that would represent remnants of the northward-subducted oceanic and continental crust (Lardeaux et al. 2001). Moreover, the rheological weakening and buoyancy of partially molten, subducted continental crust strongly enhances its decoupling with the lithospheric mantle and subsequent exhumation, as typically observed in numerical models (Duretz and Gerya 2013) and natural case studies (Labrousse et al. 2011). This would have readily triggered southward delamination of the lithospheric mantle in the context of ongoing convergence, which is supported by the fact that the orogenic front propagated southwards during the Carboniferous (Faure et al. 2009). However, the timing of exhumation of the (U)HP rocks at the base of the UGU is poorly constrained and could be as early as 360 Ma (Lardeaux et al. 2001). Thus, if this hypothesis was correct, there is a time lapse of $\geq$20 Ma between the end of continental subduction and the beginning of magmatism related to delamination (~340 Ma in the eastern FMC), which is difficult to explain since the response time between delamination and melting of the crust through asthenospheric heat advection would be much shorter, i.e., $\leq$10 Ma (Arnold et al. 2001; Depine et al. 2008).

On the other hand, the "polycyclic" model involving southward subduction during the Devonian (Fig. 12b) is consistent with arc magmatism in the Morvan and Limousin areas at 360–350 Ma and the development of the Brévenne trough as a back-arc basin (Pin and Paquette 1997; Faure et al. 2009; Lardeaux et al. 2014). It also avoids the problem of a too long time lapse between the onsets of delamination and magmatism: "retro-delamination" starting at ~350 Ma (the youngest documented subduction-related magmas being dated at 355 $\pm$ 2 Ma; Bernard-Griffiths et al. 1985) more realistically accounts for the onset of widespread magmatism at ~340 Ma in the eastern FMC. Nevertheless, this scenario implies that the asthenosphere window underneath the crust would have been much larger than in the previous one, specifically extending further north beyond the Brévenne basin, up to the Morvan area (Fig. 12b). This is problematic because in these domains, there is so far no evidence for any sequential emplacement of igneous rocks like that documented here, or even for any magmatic event younger than ~330 Ma.

More detailed investigations are therefore required to decipher between these two scenarios; at present we consider that both are equally likely to explain the observed southward lithosphere delamination and associated magmatism in the eastern FMC during the Carboniferous.

Conclusions

Variscan plutonic rocks from the eastern FMC were derived from two end-member sources: (i) a mixture of felsic lithologies (ortho- and paragneisses) from the local nappe pile (especially the Lower Gneiss Unit, in line with the predominance of late Ediacaran to early Cambrian ages in inherited zircon patterns), resulting in the formation of cordierite- and muscovite-bearing peraluminous granites (CPG and MPG); and (ii) an enriched (metasomatized) lithospheric mantle, source of the vaugnerites. The K-feldspar porphyritic, calc-alkaline granites and granodiorites (KCG) result from either interactions between these two end-members or fractionation from vaugnerite magmas.

Zircon and monazite U–Pb ages from these rocks testify for a long-lasting (~40 Ma) period of crust- and mantle-derived magmatism in the eastern FMC, as is reflected by the coeval emplacement of granites between 337.4 $\pm$ 1.0 and 298.9 $\pm$ 1.8 Ma, and vaugnerites between 335.7 $\pm$ 2.1 and 299.1 $\pm$ 1.3 Ma. Coeval and protracted crust- and mantle-derived magmatism points to the existence of a long-lived lithospheric-scale thermal anomaly, which probably formed in response to the delamination of the lithospheric mantle and asthenosphere upwelling beneath the eastern FMC during the late Carboniferous. Moreover, the spatial distribution of the dated samples indicates that delamination started at about 340 Ma in the northern part of the area and propagated southwards until 300 Ma. This may be explained either by (i) the progressive "retreat" of a lithospheric mantle slab following northward-directed subduction or (ii) "retro-delamination" of the lithosphere associated with southward-directed subduction.

References

Aït-Malek H (1997) Petrology, geochemistry and U/Pb geochronology of acid–basic associations: examples from SE Velay (French Massif Central) and western anti-Atlas (Morocco). Ph.D. thesis, University of Nancy

Alexandre P (2007) U–Pb SIMS ages from the French Massif Central and implication for the pre-Variscan tectonic evolution in Western Europe. C R Geosci 339:613–621

Alexandrov P, Floc'h JP, Cuney M, Cheilletz A (2001) Datation U–Pb à la microsonde ionique des zircons de l'unité supérieure de gneiss dans le Sud Limousin, Massif Central. C R Acad Sci Paris 332:625–632

Annen C, Sparks RSJ (2002) Effects of repetitive emplacement of basaltic intrusions on thermal evolution and melt generation in the crust. Earth Planet Sci Lett 203:937–955

Annen C, Blundy JD, Sparks RSJ (2006) The genesis of intermediate and silicic magmas in deep crust hot zones. J Petrol 47(3):505–539

Arnaud F, Burg JP (1993) Microstructures des mylonites schisteuses: cartographie des chevauchements varisques dans les Cévennes et détermination de leur cinématique. C R Acad Sci Paris 11:1441–1447

Arnold J, Jacoby WR, Schmeling H, Schott B (2001) Continental collision and the dynamic and thermal evolution of the Variscan orogenic crustal root—numerical models. J Geodynamics 31:273–291

Averbuch O, Piromallo C (2012) Is there a remnant Variscan subducted slab in the mantle beneath the Paris basin? Implications for the late Variscan lithospheric delamination process and the Paris basin formation. Tectonophysics 558–559:70–83

Ballèvre M, Le Goff E, Hébert R (2001) The tectonothermal evolution of the Cadomian belt of northern Brittany, France: a Neoproterozoic volcanic arc. Tectonophysics 331:19–43

Barbarin B (1983) Les granites carbonifères du Forez septentrional (Massif Central Français). Typologie et relations entre les différents massifs. Thèse 3e cycle, Université Clermont-Ferrand 199 p

Barbarin B (1988) Mise en évidence des différentes étapes d'un processus global de mélange de magmas acides et basiques: les interactions entre la diorite de Piolard et le monzogranite de Saint-Julien-la-Vêtre (Monts du Forez, Massif Central, France). C R Acad Sci Paris 306:129–134

Barbarin B (1992) Les granites crustaux hercyniens d'Europe Occidentale. Comparaison avec les granites S du Lachlan Fold Belt, Australie. Dualité d'origine. C R Acad Sci Paris 314:593–601

Barbarin B (1999) A review of the relationships between granitoid types, their origins and their geodynamic environments. Lithos 46(3):605–626

Barbarin B, Gerbe MC, Vitel G, Gonord H, Couette F, Lebret P (2012) Notice explicative, Carte géologique de la France (1/50,000e), feuille Firminy (nr. 744). Orléans, Bureau de Recherches Géologiques et Minières

Barbey P, Marignac C, Montel JM, Macaudière J, Gasquet D, Jabbori J (1999) Cordierite growth textures and the conditions of genesis and emplacement of crustal granitic magmas: the Velay granite (Massif Central, France). J Petrol 40(9):1425–1441

Barbey P, Villaros A, Marignac C, Montel JM (2015) Multiphase melting, magma emplacement and P-T-time path in late-collisional context: the Velay example (Massif Central, France). Bull Soc Geol Fr 186(2–3):93–116

Batias P, Duthou JL (1979) Age Viséen supérieur du granite porphyroïde de Vienne-Tournon (Massif Central français). In: Proceedings 7ème Réunion Annuelle des Sciences de la Terre, Lyon

Bé Mézème E, Cocherie A, Faure M, Legendre O, Rossi P (2006) Electron microprobe monazite geochronology of magmatic events: examples from Variscan migmatites and granitoids, Massif Central, France. Lithos 87(3–4):276–288

Beard JS, Lofgren GE (1991) Dehydration melting and water-saturated melting of basaltic and andesitic greenstones and amphibolites at 1, 3 and 6.9 kbar. J Petrol 32(2):365–401

Bernard-Griffiths J, Gebauer D, Grünenfelder M, Piboule M (1985) The tonalite belt of Limousin (French Central Massif): U–Pb zircon ages and tectonic implications. Bull Soc Geol Fr 1(4):523–529

Black R, Liégeois JP (1993) Cratons, mobile belts, alkaline rocks and continental lithospheric mantle: the Pan-African testimony. J Geol Soc Lond 150:89–98

Bogaerts M, Scaillet B, Vander Auwera J (2006) Phase equilibria of the Lyngdal granodiorite (Norway): implications for the origin of metaluminous ferroan granitoids. J Petrol 47(12):2405–2431

Bonin B (2004) Do coeval mafic and felsic magmas in post-collisional to within-plate regimes necessarily imply two contrasting, mantle and crustal, sources? A review. Lithos 78:1–24

Bouilhol P, Leyreloup AF, Delor C, Vauchez A, Monié P (2006) Relationships between lower and upper crust tectonic during doming: the mylonitic southern edge of the Velay metamorphic core complex (Cévennes-French Massif Central). Geodin Acta 19(3–4):137–153

Briand B, Piboule M, Santallier D, Bouchardon JL (1991) Geochemistry and tectonic implications of two Ordovician bimodal igneous complexes, southern French Massif Central. J Geol Soc Lond 148:959–971

Briand B, Duthou JL, Guerrot C, Chenevoy M (2002) The orthoclase lath-rich granites from Vivarais, products of a Dinantian post-tectonic magmatism; identification of a NW-Vivarais geological unit. C R Geoscience 334:741–747

Brichau S, Respaut JP, Monié P (2008) New age constraints on emplacement of the Cévenol granitoids, South French Massif Central. Int J Earth Sci 97:725–738

Brown M (2001) Crustal melting and granite magmatism: key issues. Phys Chem Earth 26(4–5):201–212

Bruguier O, Becq-Giraudon JF, Bosch D, Lancelot J (1998) Late Visean hidden basins in the internal zones of the Variscan belt: U–Pb zircon evidence from the French Massif Central. Geology 26(7):627–630

Caen-Vachette M (1979) Age cambrien des rhyolites transformées en leptynites dans la série métamorphique du Pilat (Massif Central français). C R Acad Sci Paris 289:997–1000

Caen-Vachette M, Couturié JP, Didier J (1982) Ages radiométriques des granites anatectiques et tardimigmatitique du Velay (Massif Central français). C R Acad Sci Paris 294:135–138

Caron C (1994) Les minéralisations Pb-Zn associées au Paléozoïque inférieur d'Europe méridionale. Traçage isotropique Pb-Pb des gites de l'Iglesiente (SW Sardaigne) et des Cévennes et évolution du socle encaissant par la géochronologie U–Pb, 40Ar-39Ar et K-Ar. Ph.D. thesis, University of Montpellier 288 pp

Castiñeiras P, Villaseca C, Barbero L, Romera CM (2008) SHRIMP U–Pb zircon dating of anatexis in high-grade migmatite complexes of Central Spain: implications in the Hercynian evolution of Central Iberia. Int J Earth Sci 97:35–50

Chauvet A, Volland-Tuduri N, Lerouge C, Bouchot V, Monié P, Charonnat X, Faure M (2011) Geochronological and geochemical characterization of magmatic-hydrothermal events within the Southern Variscan external domain (Cévennes area, France). Int J Earth Sci 101(1):69–86

Chelle-Michou C, Laurent O, Moyen JF, Block S, Gardien V, Paquette JL, Couzinié S (2015) New U–Pb and Hf zircon data from the eastern Massif Central: from Gondwana to Pangea in a nutshell. Géol Fr 1:37–38

Clemens JD, Darbyshire DPF, Flinders J (2009) Sources of post-orogenic calcalkaline magmas: the Arrochar and Garabal Hill-Glen Fyne complexes, Scotland. Lithos 112:524–542

Cocherie A (2007) Datations U–Pb (laser-ICPMS-MC) sur zircons et U-Th-Pb sur monazites de granitoïdes du Massif central (carte de Firminy). Rapport BRGM MMA/ISO-2007/279

Cocherie A, Be Mézème E, Legendre O, Fanning CM, Faure M, Rossi P (2005) Electron-microprobe dating as a tool for determining the closure of Th–U–Pb systems in migmatitic monazites. Am Mineral 90:607–618

Costa S, Rey P (1995) Lower crustal rejuvenation and growth during post-thickening collapse: insights from a crustal cross section through a Variscan metamorphic core complex. Geology 23(10):90–908

Coulon C, Megartsi M, Fourcade S, Maury RC, Bellon H, Louni-Hacini A, Cotten J, Coutelle A, Hermitte D (2002) Post-collisional transition from calc-alkaline to alkaline volcanism during the Neogene in Oranie (Algeria): magmatic expression of a slab breakoff. Lithos 62(3–4):87–110

Couturié JP, Caen-Vachette M (1979) Age Namurien d'un laccolite granitique différencié par gravité: le granite de la Margeride (Massif Central français). C R Acad Sci Paris 289:449–452

Couzinié S, Moyen JF, Villaros A, Paquette JL, Scarrow JH, Marignac C (2014) Temporal relationships between Mg-K mafic magmatism and catastrophic melting of the Variscan crust in the southern part of Velay Complex (Massif Central, France). J Geosci 59:69–86

Couzinié S, Laurent O, Moyen JF, Zeh A, Bouilhol P, Villaros A (2016) Post-collisional magmatism: crustal growth not identified by zircon Hf–O isotopes. Earth Planet Sci Lett 456:182–195

De la Roche H, Leterrier L, Grandclaude P, Marchal M (1980) A classification of volcanic and plutonic rocks using R1–R2 diagram and major element analyses—its relationship with current nomenclature. Chem Geol 29:183–210

De Saint-Blanquat M, Horsman E, Habert G, Morgan S, Vanderhaeghe O, Law R, Tikoff B (2011) Multiscale magmatic cyclicity, duration of pluton construction, and the paradoxical relationship between tectonism and plutonism in continental arcs. Tectonophysics 500:20–33

Denèle Y, Laumonier B, Paquette JL, Olivier P, Gleizes G, Barbey P (2014) Timing of granite emplacement, crustal flow and gneiss dome formation in the Variscan segment of the Pyrenees. In: Schulmann K, Martínez Catalán JR, Lardeaux JM, Janoušek V and Oggiano G (eds) The Variscan Orogeny: Extent, Timescale and the Formation of the European Crust. Geol Soc London Special Publications 405: 265–287

Depine GV, Andronicos CL, Phipps-Morgan J (2008) Near-isothermal conditions in the middle and lower crust induced by melt migration. Nature 452:80–83

Didier J, Lameyre J (1969) Les granites du Massif Central Français. Etude comparée des leucogranites et des granodiorites. Contrib Mineral Petrol 24:219–238

Didier J, Duthou JL, Lameyre J (1982) Mantle and crustal granites: genetic classification of orogenic granites and the nature of their enclaves. J Volc Geothermal Res 14:125–132

Didier J, Barbarin B, Gagny C, Leistel JM, Kerrien Y (1989) Notice explicative, Carte géologique de la France (1/50 000°), feuille Noirétable (nr. 695). Orléans, Bureau de Recherches Géologiques et Minières, p 72

Didier A, Bosse V, Boulvais P, Bouloton J, Paquette JL, Montel JM, Devidal JL (2013) Disturbance versus preservation of U–Th–Pb ages in monazite during fluid–rock interaction: textural, chemical and isotopic in situ study in microgranites (Velay Dome, France). Contrib Mineral Petrol 165(6):1051–1072

Do Couto D, Faure M, Augier R, Cocherie A, Rossi P, Li XH, Lin W (2015) Monazite U-Th–Pb EPMA and zircon U–Pb SIMS chronological constraints on the tectonic, metamorphic and thermal events in the inner part of the Variscan orogen, example from the Sioule series. Int J Earth Sci, French Massif Central. doi:10.1007/s00531-015-1184-0

Dostal J, Dupuy C, Leyreloup A (1980) Geochemistry and petrology of meta-igneous granulitic xenoliths in Neogene volcanic rocks of the Massif Central, France—implications for the lower crust. Earth Planet Sci Lette 50(1):31–40

Downes H, Dupuy C, Leyreloup A (1990) Crustal evolution of the Hercynian belt of Western Europe: evidence from lower-crustal granulitic xenoliths (French Massif Central). Chem Geol 83(3–4):209–231

Downes H, Shaw A, Williamson BJ, Thirlwall MF (1997) Sr, Nd and Pb isotope geochemistry of the Hercynian granodiorites and monzogranites, Massif Central, France. Chem Geol 136:99–122

Ducrot J, Lancelot J, Marchand J (1983) Datation U–Pb sur zircons de l'éclogite de la Borie (Haut-Allier, France) et conséquences sur l'évolution ante-hercynienne de l'Europe occidentale. Earth Planet Sci Lett 62:385–394

Dupraz J, Didier J (1988) Le complexe anatectique du Velay (Massif Central français): structure d'ensemble et évolution géologique. Geol Fr 4:73–88

Duretz T, Gerya TV (2013) Slab detachment during continental collision: influence of crustal rheology and interactions with lithospheric delamination. Tectonophysics 602:124–140

Duthou JL, Cantagrel JM, Didier J, Vialette Y (1984) Palaeozoic granitoids from the French Massif Central: age and origin studied by ^{87}Rb–^{87}Sr system. Phys Earth Planet Interiors 35:131–144

Duthou JL, Chenevoy M, Gay M (1994) Rb-Sr middle Devonian age of cordierite bearing migmatites from Lyonnais area (French Massif Central). C R Acad Sci Paris 319:791–796

Faure M (1995) Late orogenic carboniferous extensions in the Variscan French Massif Central. Tectonics 14(1):132–153

Faure M, Charonnat X, Chauvet A (1999) Structural map and tectonic evolution of the Cévennes para-autochtonous domain of the Hercynian belt (French Massif Central). C R Acad Sci Paris 328:401–407

Faure M, Monié P, Pin C, Maluski H, Leloix C (2002) Late Visean thermal event in the northern part of the French Massif Central: new ^{40}Ar/^{39}Ar and Rb-Sr isotopic constraints on the Hercynian syn-orogenic extension. Int J Earth Sci 91:53–75

Faure M, Bé Mézème E, Duguet M, Cartier C, Talbot JY (2005) Paleozoic tectonic evolution of medio-Europa from the example of the French Massif Central and Massif Armoricain. In: Carosi R, Dias R, Iacopini D, Rosenbaum G (eds.), The southern Variscan belt. J Virtual Explorer 19, paper 5

Faure M, Bé Mézème E, Cocherie A, Rossi P, Chemenda A, Boutelier D (2008) Devonian geodynamic evolution of the Variscan belt, insights from the French Massif Central and Massif Armoricain. Tectonics. doi:10.1029/2007TC002115

Faure M, Lardeaux JM, Ledru P (2009) A review of the pre-Permian geology of the Variscan French Massif Central. C R Geoscience 341(2–3):202–213

Féménias O, Coussaert N, Bingen B, Whitehouse M, Mercier JC, Demaiffe D (2003) A Permian underplating event in late- to post-orogenic tectonic setting. Evidence from the mafic–ultramafic layered xenoliths from Beaunit (French Massif Central). Chem Geol 199:293–315

Fernández-Suárez J, Dunning GR, Jenner GA, Gutiérrez-Alonzo G (2000) Variscan collisional magmatism and deformation in NW Iberia: constraints from U–Pb geochronology of granitoids. J Geol Soc Lond 157:565–576

Fernández-Suárez J, Gutierrez-Alonso G, Johnston ST, Jeffries TE, Pastor-Galán D, Jenner GA, Murphy JB (2011) Iberian late-Variscan granitoids: some considerations on crustal sources and the significance of "mantle extraction ages". Lithos 123:121–132

Feybesse JL, Lardeaux JM, Johan V, Tegyey M, Dufour E, Lumière B, Delfour J (1988) La série de la Brévenne (Massif Central français): une unité dévonienne charriée sur le complexe métamorphique des Monts du Lyonnais à la fin de la collision varisque. C R Acad Sci Paris 307:991–996

Finger F, Roberts MP, Haunschmid B, Schermaier A, Steyrer HP (1997) Variscan granitoids of central Europe: their typology, potential sources and tectonothermal relations. Mineral Petrol 61:67–96

François T (2009) Geochemical and geochronological constraints on the origin and emplacement of Mont-Lozère granites. M.Sc. thesis, University of Montpellier

Gardien V (1990) Reliques de grenat et de staurotide dans la série métamorphique de basse pression du Mont Pilat (Massif Central français): témoins d'une évolution tectonométamorphique polyphasée. C R Acad Sci Paris 310:233–240

Gardien V (1993) Les reliques pétrologiques de haute à moyenne pression des séries du Vivarais oriental (Est du Massif Central français). Comptes rendus de l'Académie des sciences. Série 2, Mécanique, Physique, Chimie, Sciences de l'univers. Sciences de la Terre 316:1247–1254

Gardien V, Teygey M, Lardeaux JM, Misseri M, Dufour E (1990) Crust mantle relationships in the French Variscan Belt: the example of Monts du Lyonnais unit (Eastern French Massif central). J Metam Geol 8(5):477–492

Gardien V, Thompson AB, Grujic D, Ulmer P (1995) Experimental melting of biotite + plagioclase + quartz ± muscovite assemblages and implications for crustal melting. J Geophys Res 100:15581–15591

Gardien V, Lardeaux JM, Ledru P, Allemand P, Guillot S (1997) Metamorphism during late orogenic extension; insights from the French Variscan belt. Bull Soc Geol Fr 168(3):271–286

Gardien V, Vanderhaeghe O, Arnaud N, Cocherie A, Grange M, Lécuyer C (2011) Thermal maturation and exhumation of a middle orogenic crust in the Livradois area (French Massif Central). Bull Soc Geol Fr 182(1):5–24

Gay M, Peterlongo JM, Caen-Vachette M (1981) Age radiométrique des granites en massifs allongés et en feuillets minces, syntectoniques dans les Monts du Lyonais (Massif Central français). C R Acad Sci Paris 293:993–996

Geisler T, Ulonska M, Schleicher H, Pidgeon RT, van Bronswijk W (2001) Leaching and differential recrystallization of metamict zircon under experimental conditions. Contrib Mineral Petrol 141:53–65

Gerdes A, Zeh A (2006) Combined U–Pb and Hf isotope LA-(MC) ICP-MS analyses of detrital zircons: comparison with SHRIMP and new constraints for the provenance and age of an Armorican metasediment in Central Germany. Earth Planet Sci Lett 249:47–61

Gerdes A, Zeh A (2009) Zircon formation versus zircon alteration–new insights from combined U–Pb and Lu–Hf in situ LA-ICP-MS analyses, and consequences for the interpretation of Archean zircon from the Central Zone of the Limpopo Belt. Chem Geol 261:230–243

Gray R, Pysklywec RN (2012) Geodynamic models of mature continental collision: evolution of an orogen from lithospheric subduction to continental retreat/delamination. J Geophysical Res 117(B3):B03408

Guo Z, Wilson M, Zhang M, Cheng Z, Zhang L (2013) Post-collisional, K-rich mafic magmatism in south Tibet: constraints on Indian slab-to-wedge transport processes and plateau uplift. Contrib Mineral Petrol 165:1311–1340

Harris NBW, Vance D, Ayres M (2000) From sediment to granite: timescales of anatexis in the upper crust. Chem Geol 162:155–167

Henk A, Von Blankenburg F, Finger F, Schaltegger U, Zulauf G (2000) Syn-convergent high temperature metamorphism and magmatism in the Variscides: a discussion of potential heat sources. In: Franke W, Haak V, Oncken O, Tanner D (eds) Orogenic processes: quantification and modelling in the variscan belt. Geol Soc Lond Spec Publ 179:387–399

Hou Z, Cook NJ (2009) Metallogenesis of the Tibetan collisional orogen: a review and introduction to the special issue. Ore Geol Rev 36:2–24

Isnard H (1996) Datation par la méthode U–Pb sur monazites des granites du Mont Lozère et de l'Est de la Margeride (laccolites de Chambon-le- Château et de St-Christophe d'Allier): contribution à l'histoire post-tectonique du Massif Central Français. M.Sc. thesis, University of Montpellier, 55 pp

Janoušek V, Bowes DR, Rogers G, Farrow CM, Jelínek E (2000) Modelling diverse processes in the petrogenesis of a composite Batholith: the Central Bohemian Pluton, Central European Hercynides. J Petrol 41(4):511–543

Kemp AIS, Hawkesworth CJ (2003) Granitic perspectives on the generation and secular evolution of the continental crust. In: Rudnick RL (ed) The crust. Treatise on geochemistry. Elsevier-Pergamon, Oxford, pp 349–410

Kober B, Kalt A, Hanel M, Pidgeon RT (2004) SHRIMP dating of zircons from high-grade metasediments of the Schwarzwald/SW-Germany and implications for the evolution of the Moldanubian basement. Contrib Mineral Petrol 147:330–345

Kosztolanyi C (1971) Géochronologie des gisements uranifères français par la méthode uranium-plomb. Influence du déséquilibre radioactif sur les résultats. Ph.D. thesis, University of Nancy 279 pp

Kroner U, Romer RL (2013) Two plates—many subduction zones: the Variscan orogeny reconsidered. Gondwana Res 24(1):298–329

Labrousse L, Prouteau G, Ganzhorn AC (2011) Continental exhumation triggered by partial melting at high pressure. Geology 39(12):1171–1174

Lafon JM (1986) Géochronologie U-Pb appliquée à deux segments du massif central français, le Rouergue oriental et le Limousin central. Thèse de l'Université de Montpellier, p 152

Lafon JM, Respaut JP (1988) Géochronologie U–Pb et leucogranites varisques : cas des massifs de Grandrieu (Lozère) et de la Porcherie (Limousin), Massif Central français. Bull Minér 111:225–237

Lardeaux JM, Ledru P, Daniel I, Duchène S (2001) The Variscan French Massif Central—a new addition to the ultra-high pressure metamorphic "club": exhumation processes and geodynamic consequences. Tectonophysics 332:143–168

Lardeaux JM, Schulmann K, Faure M, Janoušek V, Lexa O, Skrzypek E, Edel JB, Tipska P (2014) The moldanubian zone in the French Massif Central, Vosges/Schwarzwald and Bohemian Massif revisited: differences and similarities. Geol Soc Lond Spec Publ 405(1):7–44

Laurent O, Doucelance R, Martin H, Moyen JF (2013) Differentiation of the late-Archaean sanukitoid series and some implications for crustal growth: insights from geochemical modelling on the Bulai pluton, Central Limpopo Belt, South Africa. Precambrian Res 227:186–203

Laurent O, Martin H, Moyen JF, Doucelance R (2014a) The diversity and evolution of late-Archean granitoids: evidence for the onset of modern-style plate tectonics between 3.0 and 2.5 Ga. Lithos 205:208–235

Laurent O, Rapopo M, Stevens G, Moyen JF, Martin H, Doucelance R, Bosq C (2014b) Contrasting petrogenesis of Mg–K and Fe–K granitoids and implications for post-collisional magmatism: case study from the Late-Archean Matok pluton (Pietersburg block, South Africa). Lithos 196–197:131–149

Ledru P, Lardeaux JM, Santallier D, Autran A, Quenardel JM, Floch JP, Lerouge G, Maillet N, Marchand J, Ploquin A (1989) Où sont les nappes dans le Massif central français ? Bulletin de la Société Geologique de France 8:605–618

Ledru P, Courrioux G, Dallain C, Lardeaux JM, Montel JM, Vanderhaeghe O, Vitel G (2001) The Velay dome (French Massif Central): melt generation and granite emplacement during orogenic evolution. Tectonophysics 342:207–237

Leloix C, Faure M, Feybesse JL (1999) Hercynian polyphase tectonics in the northeast French Massif Central: the closure of the Brévenne Devonian-Dinantian rift. Int J Earth Sci 88:409–421

Liégeois JP, Navez J, Hertogen J, Black R (1998) Contrasting origin of post-collisional high-K calc-alkaline and shoshonitic versus alkaline and peralkaline granitoids. The use of sliding normalization. Lithos 45:1–28

Linnemann U, McNaughton NJ, Romer RL, Gehmlich M, Drost K, Tonk C (2004) West African provenance for Saxo-Thuringia (Bohemian Massif): did Armorica ever leave pre-Pangean Gondwana? U/Pb-SHRIMP zircon evidence and the Nd isotopic record. Int J Earth Sci 93:683–705

Linnemann U, Gerdes A, Drost K, Buschmann B (2007) The continuum between Cadomian orogenesis and opening of the Rheic Ocean: Constraints from LA-ICP-MS U–Pb zircon dating and analysis of plate-tectonic setting (Saxo-Thuringian zone, northeastern Bohemian Massif, Germany). In: Linnemann U, Nance RD, Kraft P, Zulauf G (eds) the evolution of the Rheic Ocean: From Avalonian-Cadomian active margin to Alleghenian-Variscan collision. Geological Society of America Special Paper vol 423, pp 61–96

Linnemann U, Gerdes A, Hofmann M, Marko L (2014) The Cadomian Orogen: neoproterozoic to Early Cambrian crustal growth and orogenic zoning along the periphery of the West African Craton—Constraints from U–Pb zircon ages and Hf isotopes (Schwarzburg Antiform, Germany). Precambrian Res 244:236–278

Lotout C, Pitra P, Poujol M, van den Driessche J (in press) Ordovician magmatism in the Lévézou massif (French Massif Central): tectonic and geodynamic implications. Int J Earth Sci. doi:10.1007/s00531-016-1387-z

Ludwig KR (2008) Isoplot 3.70, a geochronological toolkit for microsoft excel. Berkeley Geochronology Central Special Publication No. 4

Magni V, Faccenna C, van Hunen J, Funiciello F (2013) Delamination versus break-off: the fate of continental collision. Geophys Res Lett 40:285–289

Malavieille J, Guilhot P, Costa S, Lardeaux JM, Gardien V (1990) Collapse of the thickened Variscan crust in the French Massif Central: Mont Pilat extensional shear zone and St. Etienne Late Carboniferous basin. Tectonophysics 177(1–3):139–149

Matte P (1986) Tectonics and plate tectonics model for the Variscan belt of Europe. Tectonophysics 126:329–374

Melleton J, Faure M, Cocherie A (2009) Monazite U–Th/Pb chemical dating of the Early Carboniferous syn-kinematic MP/MT metamorphism in the Variscan French Massif Central. Bull Soc Geol Fr 180(3):283–292

Melleton J, Cocherie A, Faure M, Rossi P (2010) Precambrian protoliths and Early Paleozoic magmatism in the French Massif Central: U–Pb data and the North Gondwana connection in the west European Variscan belt. Gondwana Res 17(1):13–25

Mercier L, Lardeaux JM, Davy P (1991) On the tectonic significance of retrograde P–T–t paths in eclogites of the French Massif Central. Tectonics 10(1):131–140

Mezger K, Krogstad EJ (1997) Interpretation of discordant U–Pb zircon ages—an evaluation. J Metamorphic Geol 15:127–140

Mintrone M (2015) Le Massif Central avant la chaîne Varisque: caractérisation des orthogneiss du début du Primaire. Travail d'Étude et de Recherche, University of Clermont-Ferrand, France, p 31

Montel JM, Weisbrod A (1986) Characteristics and evolution of "vaugneritic magmas": an analytical and experimental approach, on the example of the Cévennes Médianes (French Massif Central). Bull Minéral 109:575–587

Montel JM, Marignac C, Barbey P, Pichavant M (1992) Thermobarometry and granite genesis: the Hercynian low-P, high-T Velay anatectic dome (French Massif Central). J Metamorph Geol 10:1–15

Mougeot R, Respaut JP, Ledru P, Marignac C (1997) U–Pb chronology on accessory minerals of the Velay anatectic dome (French Massif Central). Eur J Mineral 9:141–156

Moyen JF, Laurent O, Chelle-Michou C, Couzinié S, Vanderhaeghe O, Zeh A, Villaros A, Gardien G (in press) Collision versus subduction-related magmatism: two contrasting ways of granite formation and implications for crustal growth. Lithos doi:10.1016/j.lithos.2016.09.018

Nance DR, Murphy BJ (1994) Contrasting basement isotopic signatures and the palinspastic restoration of peripheral orogens: examples from the Neoproterozoic Avalonian-Cadomian Belt. Geology 22:617–620

Nance DR, Murphy BJ, Strachan RA, D'Lemos RS, Taylor GK (1991) Late Proterozoic tectonostratigraphic evolution of the Avalonian and Cadomian terranes. Precambrian Res 53:41–78

Nance RD, Murphy JB, Keppie JD (2002) A Cordilleran model for the evolution of Avalonia. Tectonophysics 352:11–31

Nance RD, Gutierrez-Alonso G, Keppie JD, Linnemann U, Murphy JB, Quesada C, Strachan RA, Woodcock NH (2010) Evolution of the Rheic Ocean. Gondwana Res 17:194–222

Nelson KD et al (1996) Partially molten middle crust beneath southern Tibet: synthesis of project INDEPTH results. Science 274:1684–1688

Paquette LD, Monchoux P, Couturier M (1995) Geochemical and isotopic study of a norite-eclogite transition in the European Variscan belt: implications for U–Pb zircon systematics in metabasic rocks. Geochim Cosmochim Acta 59(8):1611–1622

Patiño-Douce AE, Beard JS (1995) Dehydration-melting of biotite gneiss and quartz amphibolite from 3 to 15 kbar. J Petrol 36:707–738

Patiño-Douce AE, Beard JS (1996) Effects of P, $f(O_2)$ and Mg/Fe ratio on dehydration-melting of model metagreywackes. J Petrol 37:999–1024

Patiño-Douce AE, Harris N (1998) Experimental constraints on Himalayan anatexis. J Petrol 39(4):689–710

Patiño-Douce AE, Johnston AD (1991) Phase equilibria and melt productivity in the pelitic system: implications for the origin of peraluminous granitoids and aluminous granulites. Contrib Mineral Petrol 107:202–218

Peccerillo A, Taylor SR (1976) Geochemistry of Eocene calc-alkaline volcanic rocks from the Kastamonu area, northern Turkey. Contrib Mineral Petrol 58:63–81

Petford N, Gallagher K (2001) Partial melting of mafic (amphibolitic) lower crust by periodic influx of basaltic magma. Earth Planet Sci Lett 193:483–489

Petford N, Cruden AR, McCaffrey KJW, Vigneresse JL (2000) Granite magma formation, transport and emplacement in the Earth's crust. Nature 408:669–673

Pickering JM, Johnston AD (1998) Fluid-absent melting behavior of a two-mica metapelite: experimental constraints on the origin of black hills granite. J Petrol 39(10):1787–1804

Pin C (1979a) Âge de 482 Ma des roches orthodérivées du groupe leptyno-amphibolique de Marvejols (Lozère, Massif central français) déterminé par la méthode U–Pb sur zircons. C R Acad Sci Paris Ser II 288:291–294

Pin C (1979b) Géochronologie U–Pb et microtectonique des séries métamorphiques anté-stéphaniennes de l'Aubrac et de la région de Marvejols (Massif Central). Ph.D. thesis, University of Montpellier, p 205

Pin C, Duthou J (1990) Sources of Hercynian granitoids from the French Massif Central: inferences from Nd isotopes and consequences for crustal evolution. Chem Geol 83:281–296

Pin C, Lancelot J (1982) U–Pb dating of an early paleozoic bimodal magmatism in the French Massif Central and of its further metamorphic evolution. Contrib Mineral Petrol 79:1–12

Pin C, Paquette JL (1997) A mantle-derived bimodal suite in the Hercynian Belt: Nd isotope and trace element evidence for a subduction-related rift origin of the Late Devonian Brévenne metavolcanics, Massif Central (France). Contrib Mineral Petrol 129:222–238

Pin C, Paquette JL (2002) Sr-Nd isotope and trace element evidence for a Late Devonian active margin in northern Massif Central (France). Geodin Acta 15:63–77

Pin C, Binon M, Belin JM, Barbarin B, Clemens JD (1990) Origin of microgranular enclaves in granitoids: Equivocal Sr-Nd Evidence From Hercynian Rocks in the Massif Central (France). J Geophysical Res 95(B11):17821

Rapp RP, Watson EB (1995) Dehydration melting of metabasalt at 8–32 kbar: implications for continental growth and crust–mantle recycling. J Petrol 36(4):891–931

Rapp RP, Watson EB, Miller CF (1991) Partial melting of amphibolite/eclogite and the origin of Archaean trondhjemites and tonalites. Precambrian Res 51:1–25

Respaut JP (1984) Géochronologie et géochimie isotopique U–Pb de la minéralisation uranifère de la mine des Pierres Plantées (Lozère) et de son encaissant: le massif granitique de la Margeride. Ph.D. thesis, University of Montpellier

R'Kha Chaham K, Couturié JP, Duthou JL, Fernandez A, Vitel G (1990) L'orthogneiss œillé de l'Arc de Fic : un nouveau témoin d'âge cambrien d'un magmatisme hyper alumineux dans le Massif Central français. C R Acad Sci Paris 311:845–850

Rossi P, Pin C (2008) Les magmatismes paléozoïques. La chaîne Varisque, Géochroniques 105:53–56

Sabatier H (1991) Vaugnerites: special lamprophyre-derived mafic enclaves in some Hercynian granites from Western and Central Europe. In: Didier J, Barbarin B (eds) Enclaves and granite petrology. Elsevier, Amsterdam, pp 63–81

Saint-Joanis R (1975) Étude géologique du socle cristallin du Bas-Livradois (Massif central français) dans le périmètre de la feuille d'Issoire. Ph.D. thesis, Université Blaise Pascal, Clermont-Ferrand

Scarrow JH, Bea F, Monter PG, Molina JF (2008) Shoshonites, vaungerites and potassic lamprophyres: similarities and differences between 'ultra'-high-K rocks. Trans R Soc Edimburgh 99:159–175

Schilling FR, Partzsch GM (2001) Quantifying partial melt fraction in the crust beneath the central Andes and the Tibetan Plateau. Phys Chem Earth 26:239–246

Schulmann K, Lexa O, Štípská P, Racek M, Tajčmanová L, Konopásek J, Edel JB, Pescler A, Lehmann J (2008) Vertical extrusion and horizontal channel flow of orogenic lower crust: key exhumation mechanisms in large hot orogens? J Metamorph Geol 26:273–297

Schulz B (2014) Early Carboniferous P-T path from the Upper Gneiss Unit of Haut-Allier (French Massif Central)–reconstructed by geothermobarometry and EMP-Th–U–Pb monazite dating. J Geosci, pp 327–349

Singh J, Johannes W (1996) Dehydration melting of tonalites. 2. Compositions of melts and solids. Contrib Mineral Petrol 125:26–44

Sisson T, Ratajeski K, Hankins W, Glazner A (2005) Voluminous granitic magmas from common basaltic sources. Contrib Mineral Petrol 148:635–661

Skjerlie KP, Johnston AD (1996) Vapour-absent melting from 10 to 20 kbar of crustal rocks that contain multiple hydrous phases: implications for anatexis in the deep to very deep continental crust and active continental margins. J Petrol 37:661–691

Solgadi F, Moyen JF, Vanderhaeghe O, Sawyer EW, Reisberg L (2007) The relative roles of crustal anatexis and mantle-derived magmas: generation of Synorogenic, Hercynian granites in the Livradois area, French Massif Central. Can Mineral 45:581–606

Stampfli GM, Hochard C, Vérard C, Wilhem C, von Raumer J (2013) The formation of Pangea. Tectonophysics 593:1–19

Stussi JM, De la Roche A (1984) Le magmatisme orogénique granitique de la chaîne varisque française. Typologie chimique et répartition spatiale. C R Acad Sci Paris (Série 2) 298:43–48

Supply P (1981) Géochronologie U–Pb et pétrologie des enclaves granulitiques de Bournac (Massif Central), M.Sc. thesis, University of Montpellier

Tatsumi Y, Suzuki T (2009) Tholeiitic versus calc-alkalic differentiation and evolution of arc crust: constraints from melting experiments on a basalt from the Izu–Bonin–Mariana Arc. J Petrol 50(8):1575–1603

Turpin L, Velde D, Pinte G (1988) Geochemical comparison between minettes and kersantites from the Western European Hercynian orogen: trace element and Pb–Sr–Nd isotope constraints on their origin. Earth Planet Sci Lett 87:73–86

Turpin L, Cuney M, Friedrich M, Bouchez JL, Aubertin M (1990) Meta-igneous origin of Hercynian peraluminous granites in N.W. French Massif Central: implications for crustal history reconstructions. Contrib Mineral Petrol 104:163–172

van Hunen J, Allen MB (2011) Continental collision and slab break-off: a comparison of 3-D numerical models with observations. Earth Planet Sci Lett 302(1–2):27–37

Vanderhaeghe O (2009) Migmatites, granites and orogeny: flow modes of partially molten rocks and magmas associated with melt/solid segregation in orogenic belts. Tectonophysics 477:119–134

Vanderhaeghe O (2012) The thermal–mechanical evolution of crustal orogenic belts at convergent plate boundaries: a reappraisal of the orogenic cycle. J Geodynamics 56–57:124–145

Vanderhaeghe O, Duchêne S (2010) Crustal-scale mass transfer, geotherm and topography at convergent plate boundaries. Terra Nova 22:315–323

Vanderhaeghe O, Teyssier C (2001) Partial melting and flow of orogens. Tectonophysics 342:451–472

Vanderhaeghe O, Burg JP, Teyssier C (1999) Exhumation of migmatites in two collapsed orogens: Canadian cordillera and French Variscides. In: Ring U, Brandon MT, Lister GS, Willett SD (eds) Exhumation processes: normal faulting, ductile flow and erosion. Geological Society of London Special Publication vol 154, pp 181–204

Vermeesch P (2012) On the visualisation of detrital age distributions. Chem Geol 312–313:190–194

Vielzeuf D, Holloway JR (1988) Experimental determination of the fluid-absent melting relations in the pelitic system. Contrib Mineral Petrol 98:257–276

Vielzeuf D, Montel JM (1994) Partial melting of metagreywackes. 1. Fluid-absent experiments and phase relationships. Contrib Mineral Petrol 117:375–393

von Raumer JF, Stampfli GM, Borel G, Bussy F (2002) Organization of pre-Variscan basement areas at the north-Gondwanan margin. Int J Earth Sci 91:35–52

von Raumer JF, Finger F, Veselá P, Stampfli GM (2013) Durbachites-Vaugnerites—a geodynamic marker in the central European Variscan orogen. Terra Nova. doi:10.1111/ter.12071

Walker BA, Miller CF, Claiborne LL, Wooden JL, Miller JS (2007) Geology and geochronology of the Spirit Mountain batholith, southern Nevada: implications for timescales and physical processes of batholith construction. J Volcanol Geothermal Res 167(1–4):239–262

Watkins JM, Clemens JD, Treloar PJ (2007) Archaean TTGs as sources of younger granitic magmas: melting of sodic metatonalites at 0.6–1.2 GPa. Contrib Mineral Petrol 154:91–110

Watson EB, Harrison TM (1983) Zircon saturation revisited—temperature and composition effects in a variety of crustal magma types. Earth Planet Sci Lett 64:295–304

Williamson BJ, Downes H, Thirlwall MF (1992) The relationship between crustal magmatic underplating and granite genesis: an example from the Velay granite complex, Massif Central, France. Trans R Soc Edinb Earth Sci 83:235–245

Williamson BJ, Shaw A, Downes H, Thirlwall MF (1996) Geochemical constraints on the genesis of Hercynian two-mica leucogranites from the Massif Central, France. Chem Geol 127:25–42

Williamson B, Downes H, Thirlwall M, Beard A (1997) Geochemical constraints on restite composition and unmixing in the Velay anatectic granite, French Massif Central. Lithos 40(2–4):295–319

Wolf MB, Wyllie PJ (1994) Dehydration-melting of amphibolite at 10 kbar: the effects of temperature and time. Contrib Mineral Petrol 115:369–383

Zeh A, Gerdes A (2010) Baltica- and Gondwana-derived sediments in the Mid-German Crystalline Rise (Central Europe): implications for the closure of the Rheic ocean. Gondwana Res 17:254–263

Zeh A, Brätz H, Millar IL, Williams IS (2001) A combined zircon SHRIMP and Sm-Nd isotope study on high-grade paragneisses from the Mid-German Crystalline Rise: evidence for northern Gondwanan and Grenvillian provenance. J Geol Soc Lond 158:983–994